SEMMELWEIS EGYETEM

DOKTORI ISKOLA

Ph.D. értekezések

2950.

ANKER PÁLMA

Bőrgyógyászat és venerológia

című program

Programvezető: Dr. Sárdy Miklós, egyetemi tanár

Témavezető: Dr. Medvecz Márta, egyetemi docens

MULTIMODAL SKIN IMAGING ASSESSMENT OF RARE, INHERITED DISORDERS

PhD thesis

Pálma Anker, MD

Károly Rácz Doctoral School of Clinical Medicine

Semmelweis University

Supervisor: Márta Medvecz, MD, PhD

Official reviewers: Péter Reismann MD, PhD, Eszter Szlávicz MD, PhD

Head of the Complex Examination Committee: Prof. Miklós Csala, MD, PhD, DSc

Members of the Complex Examination Committee: Barbara Molnár-Érsek, PhD, Eszter Baltás, MD, PhD

Budapest
2023

TABLE OF CONTENTS

1. INTRODUCTION 6

1.1. Rare diseases and genodermatoses 6

1.2. Ichthyoses 6

1.3. Fabry Disease 10

1.3.1. Epidemiology 10

1.3.2. Pathogenesis 10

1.3.3. Diagnosis 11

1.3.4. Angiokeratomas in Fabry disease 12

1.3.5. Other cutaneous signs 13

1.3.6. Disease-specific therapy 14

1.4. Imaging of the skin 14

1.4.1. Clinical photography 14

1.4.2. Dermoscopy 15

1.4.3. Multispectral imaging 15

1.4.4. Nonlinear microscopy 15

2. OBJECTIVES 17

3. METHODS 18

3.1. Visualization of keratin with multispectral imaging and nonlinear microscopy in a rare keratinopathic ichthyosis 18

3.1.1. Patient and genetical analysis 18

3.1.2. Multispectral imaging 18

3.1.3. Nonlinear microscopy and conventional histology 19

3.2. Assessment of angiokeratomas in Fabry disease 19

3.2.1. Patients and diagnosis 19

3.2.2. Dermoscopy 20

3.2.3. Multispectral imaging 20

3.2.4. Nonlinear microscopy and conventional histology 20

3.2.5. Ethical statement 20

4. RESULTS 22

4.1. Case presentation of a rare keratinopathic ichthyosis and assessment with multispectral imaging and nonlinear microscopy 22

4.1.1. Case presentation 22

4.1.2. Multispectral imaging 24

4.1.3. Nonlinear microscopy 26

4.2. Assessment of angiokeratomas and other cutaneous signs in Fabry Disease 30

4.2.1. Patient cohort, extracutaneous manifestations 30

4.2.2. Clinical presentation of angiokeratomas 31

4.2.3. Other cutaneous manifestations 37

4.2.4. Dermoscopic features of angiokeratomas 38

4.2.5. Dermoscopic features of other vascular structures 41

4.2.6. Nonlinear microscopy of angiokeratomas 42

4.2.7. Multispectral imaging 44

5. DISCUSSION 46

6. CONCLUSIONS 54

7. SUMMARY 56

8. REFERENCES 57

9. BIBLIOGRAPHY OF THE CANDIDATE'S PUBLICATIONS 63

10. ACKNOWLEDGEMENTS 65

LIST OF ABBREVIATIONS

ACDU: angiokeratoma corporis diffusum universale

ADHD: attention deficit hyperactivity disorder

AEI: annular epidermolytic ichthyosis

AGAL: alpha-galactosidase A enzyme

AREI: autosomal recessive epidermolytic ichthyosis

aSICI: acral self-improving collodion ichthyosis

BSI: bathing suit ichthyosis

CDPX2: Conradi-Hunerman-Happle syndrome

CIE: congenital ichthyosiform erythroderma

CRIE: congenital reticular ichthyosiform erythroderma

EI: epidermolytic ichthyosis

EKV: erythrokeratoderma variabilis

EM: electronmicroscopy

ERT: enzyme replacement therapy

H&E: hematoxylin and eosin

HI: Harlequin-ichthyosis

IOD: integrated optical density

IPS: ichthyosis-prematurity syndrome

IV: ichthyosis vulgaris

LB: lamellar bodies

LI: lamellar ichthyosis

FD: Fabry disease

KID: Keratitis-ichthyosis-deafness syndrome

KLICK: Keratosis linearis with ichthyosis congenita and sclerosing keratoderma syndrome

KPI: keratinopathic ichthyosis

MEDNIK: Intellectual disability-enteropathy-deafness-peripheral neuropathy-ichthyosis-keratodermia syndrome

MSI: multispectral imaging

NLM: nonlinear microscopy

NISCH: Neonatal ichthyosis-sclerosing cholangitis syndrome

NTS: Netherton syndrome

PPK: palmoplantar keratoderma

PSD: peeling skin syndrome

ROI: region of interest

SEI: superficial epidermolytic ichthyosis

SHG: second harmonic generation

SICI: self-improving collodion ichthyosis

SLS: Sjögren-Larsson syndrome

STS: steroid sulfatase enzyme

TGM-1: transglutaminase-1 enzyme

TPF: two-photon absorption fluorescence

TTD: trichothiodystrophy

XLRI: X-linked recessive ichthyosis

1. INTRODUCTION

1.1. Rare diseases and genodermatoses

The definition of rare diseases is not exact, as it ranges with jurisdictions (1). In the Europen Union the prevalence threshold for rare diseases is 1:2000. Up to this point, 5000–8000 distinct rare diseases have been recorded in the medical literature and further diseases are continuously reported (1). Recent scientific and technical advancements that improved our genetic, molecular, and biochemical understanding also led to increased awareness of rare diseases (1). Approximately 80% of rare diseases are genetically inherited. Genodermatoses are inherited disorders that present characteristic cutaneous signs with or without multisystemic involvement. As of now, 560 genodermatoses have been identified. Due to their clinical heterogeneity and rarity, the diagnosis may be difficult to establish, common dermatological signs include disorders of cornification, pigmentation, vascularisation and blistering (2).

1.2. Ichthyoses

Ichthyoses are a group of rare inherited or acquired skin diseases characterized by disorders of cornification resulting to various extent in scaling, hyperkeratosis and erythroderma as well as palmoplantar hyperkeratosis or hyperlinearity (3). The term "ichthyosis" comes from the Greek word "ichthys," which means fish, as the scaling on the skin can resemble fish scales. Inherited ichthyoses are considered classical genodermatoses that follow a monogenic autosomal or X-linked inheritance affecting genes that participate in the differentiation or metabolism of keratinocytes (3). In order to maintain the proper function of the skin barrier, the precise, layer-specific expression of proteins is essential, as a result of which the cells undergo dramatic morphological and biochemical changes (*Figure 1.*). This finely regulated process is called terminal differentiation, when keratinocytes become nuclear- and organelle-depleted corneocytes. The basal cell row of the epidermis is attached to the basement membrane by hemidesmosomes, their main intermediate filament is keratin 5/14, which is replaced suprabasally by the expression of keratin 1/10 and keratin 2. In the suprabasal cells, structural proteins are associated with the plasma membrane through the mediation of transglutaminases. The granular layer is characterized by specific organelles, namely keratohyaline granules containing profilaggrin and lamellar bodies. These organelles play

a vital role in the formation of the corneocyte lipid envelope and intercellular lipid layer, which are essential for maintaining the integrity of the skin barrier (4). Cells in the uppermost layers undergo a tissue-specific form of programmed cell death. Here the primary constituents of corneocytes include keratin, filaggrin, and loricrin. The organelle-depleted corneocytes are connected through modified demosomes, called corneodemosomes. These proteins contribute to the formation of the cornified cell envelope. At the end of the differentiation process of cornified cells, serine and cysteine proteases cleave corneodesmosomes, enabling desquamation (5).

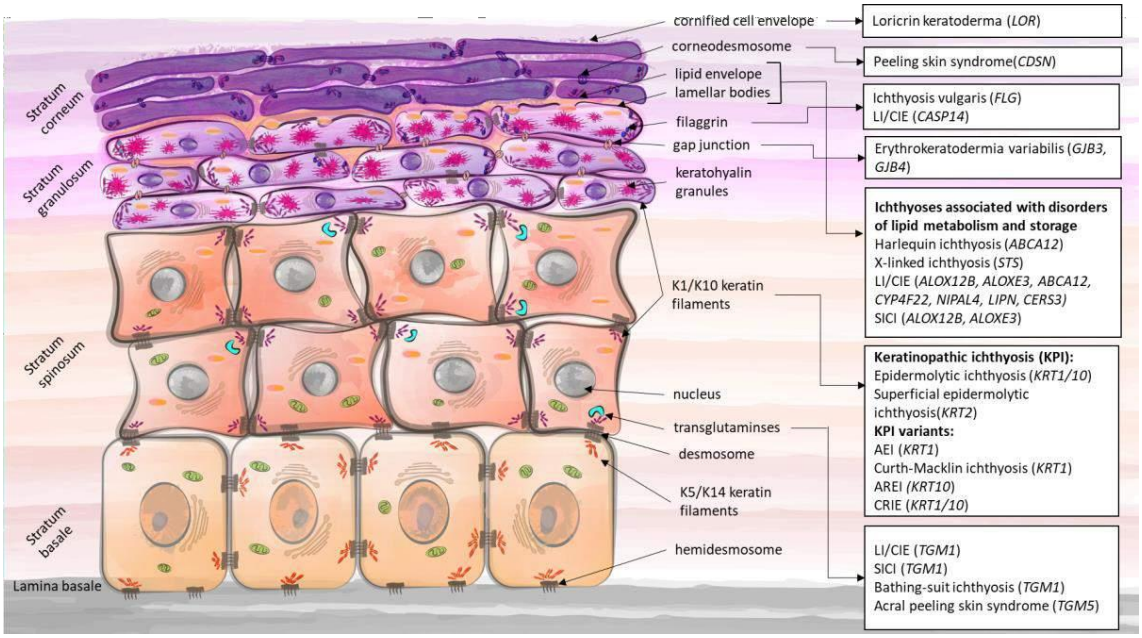

Figure 1. *Layers of the epidermis, the key components of cornification in connection to different types of ichthyoses (affected genes in brackets). Abbreviations: LI: lamellar ichthyosis; CIE: congenital ichthyosiform erythroderma; AEI: annular epidermolytic ichthyosis; AREI: autosomal recessive epidermolytic ichthyosis; CRIE: congenital reticular ichthyosiform erythroderma; SICI: self-improving collodion ichthyosis (6).*

In general, mutations of structural proteins show a predominantly dominant inheritance, while enzymes and transporters participating in keratinocyte differentiation show a recessive pattern of inheritance (6). There are over 20 different types of ichthyoses (7), mutations in more than 50 genes have been described (3). Non-syndromic ichthyoses only affect the skin and can be further categorized into common and uncommon types, while syndromic forms are classified based on the accompanying symptoms (3). From an

epidemiological perspective, the most commonly encountered forms of non-syndromic ichthyoses include ichthyosis vulgaris and the non-syndromic form of X-linked ichthyosis. Rare entities comprise members of the autosomal recessive congenital ichthyosis (ARCI) group as well as keratinopathic ichthyoses (KPI) (5).

KPI are attributed to mutations of the layer-specific keratin genes present in the suprabasal keratinocytes that lead to skin fragility. Epidermolytic ichthyosis (EI, OMIM: 113800), previously known as epidermolytic hyperkeratosis and bullous congenital ichthyosiform erythroderma of Brocq, results from dominant negative mutations in the genes encoding keratin 1 and 10 (*KRT1, KRT10*). Initiative signs at birth include erythroderma and blistering followed by hyperkeratosis to a variable degree. Typically, *KRT1* mutations are associated with palmoplantar keratoderma (PPK). Mutations of *KRT2* are associated with superficial EI, previously known as ichthyosis bullosa of Siemens (3).

In the last two decades, several disease-causing mutations have been identified in the background of inherited ichthyoses. Molecular genetic testing has become widely available and is now a basic tool to confirm the diagnosis of ichthyoses. For decades, Sanger sequencing has been the gold standard of genetic testing, whereby a known disease-causing gene is analyzed. In the case of those genodermatoses, where the genotype-phenotype correlation is well established, the assessment of the target gene can confirm the diagnosis, otherwise it is an expensive and time-consuming approach. Panel testing, such as next-generation sequencing, can help identify various mutations, which is particularly valuable when dealing with rare forms of ichthyoses where genotype-phenotype correlation is not well established. Nevertheless, prior to this stage, a thorough clinical examination and other diagnostic procedures, including conventional histology or immunohistochemistry should be employed to narrow down the diagnosis (*Figure 2.*) (5, 8).

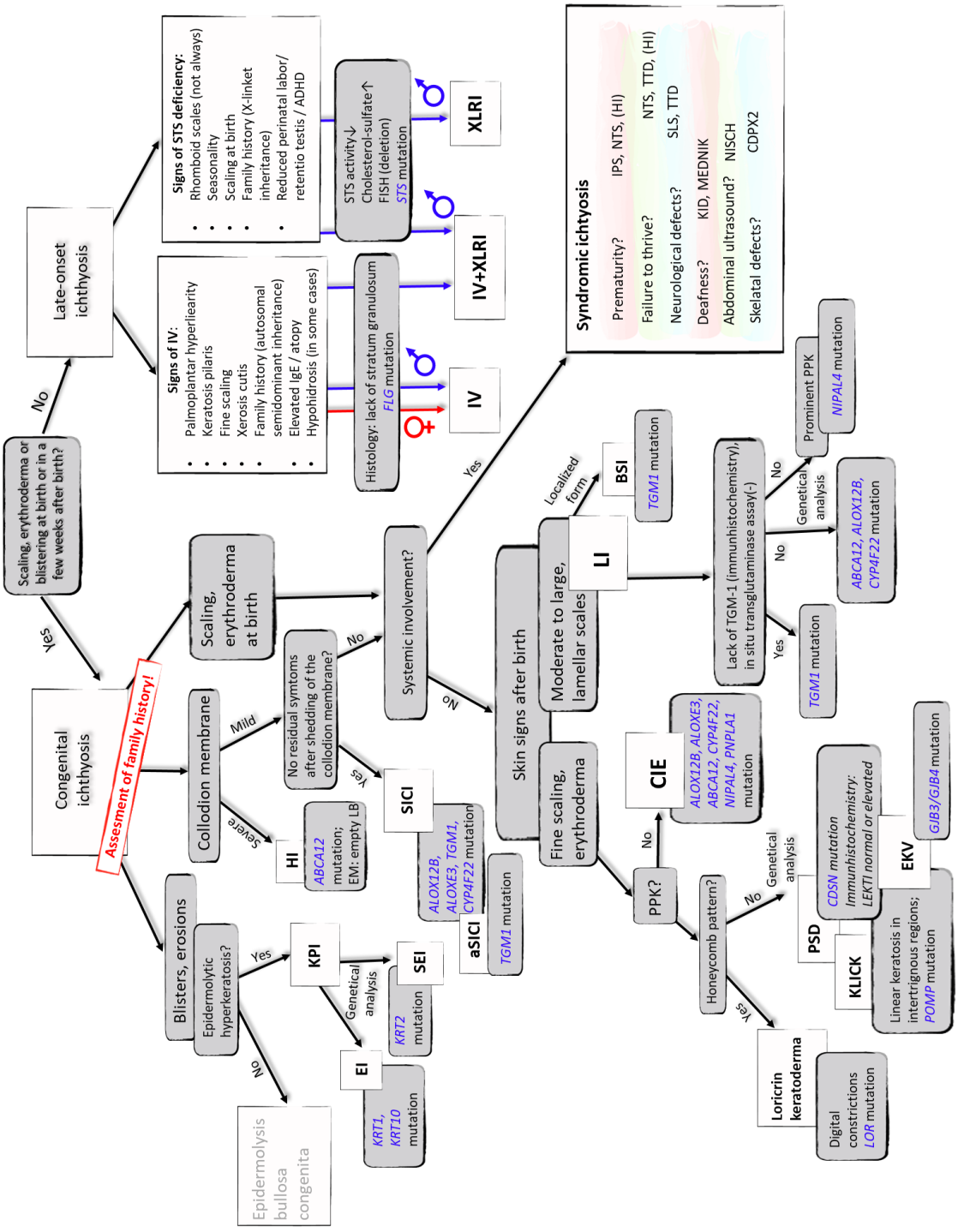

Figure 2.: *Diagnostic workup for ichthyoses. Abbreviations: ADHD: attention deficit hyperactivity disorder, aSICI: acral self-improving collodion ichthyosis, BSI: bathing suit ichthyosis, CDPX2: Conradi-Hunerman-Happle syndrome, CIE: congenital ichthyosiform erythroderma, EI: epidermolytic ichthyosis, EKV: erythrokeratoderma variabilis, EM: electron microscopy, HI: Harlequin-ichthyosis, IPS: ichthyosis-prematurity syndrome, IV: ichthyosis vulgaris, KID: Keratitis-ichthyosis-deafness syndrome, KLICK: Keratosis linearis with*

ichthyosis congenita and sclerosing keratoderma syndrome, KPI: keratinopathic ichthyosis, LB: lamellar bodies, LI: lamellar ichthyosis, MEDNIK: Intellectual disability-enteropathy-deafness-peripheral neuropathy-ichthyosis-keratodermia syndrome, NISCH: Neonatal ichthyosis-sclerosing cholangitis syndrome, NTS: Netherton syndrome, PPK: palmoplantar keratoderma, PSD: peeling skin syndrome, SEI: superficial epidermolytic ichthyosis, SICI: self-improving collodion ichthyosis, SLS: Sjögren-Larsson syndrome, STS: steroid sulfatase enzyme, TGM-1: transglutaminase-1 enzyme, TTD: trichothiodystrophy, XLRI: X-linked recessive ichthyosis (9)

To date, curative interventions for congenital ichthyoses remain elusive, however, several symptomatic approaches have been developed for management. The early diagnosis of congenital ichthyoses holds great significance for several reasons. Firstly, timely identification allows for appropriate and prompt management, thereby improving the quality of life for affected individuals. Early interventions can help alleviate symptoms, prevent complications, and optimize long-term outcomes. Genetic counseling plays a vital role in the context of congenital ichthyoses as it provides valuable information about the genetic basis of the condition, its inheritance pattern, and the likelihood of recurrence in future pregnancies. Furthermore, genetic counseling aids in understanding the underlying molecular mechanisms of congenital ichthyoses, facilitating research efforts and the development of novel therapeutic strategies. By elucidating the genetic components involved, genetic counseling can contribute to the advancement of personalized medicine approaches, such as gene and cell therapy (10).

1.3. Fabry Disease

1.3.1. Epidemiology

Fabry disease (FD, OMIM 301500), is an X-linked inherited disorder that affects glycosphingolipid metabolism. The initial estimated prevalence of FD in males was 1 in 40,000 (11). However, recent newborn screening studies indicate a higher incidence of the disease, reported between 1:3,100-1:1,250 (12). In Hungary, newborn screening studies showed an incidence of 1:13,341 (13). This variation in prevalence and incidence may be attributed to the clinical heterogeneity of the disease (12).

1.3.2. Pathogenesis

FD is caused by mutations in the *GLA* gene, which impairs alpha-galactosidase A enzyme (AGAL) activity and results in the lysosomal accumulation of Gb3 in various cells

including the endothelium, vascular smooth muscle, myocardium and corneal epithelium. This leads to diverse clinical symptoms due to progressive organ damage (Figure 3.).

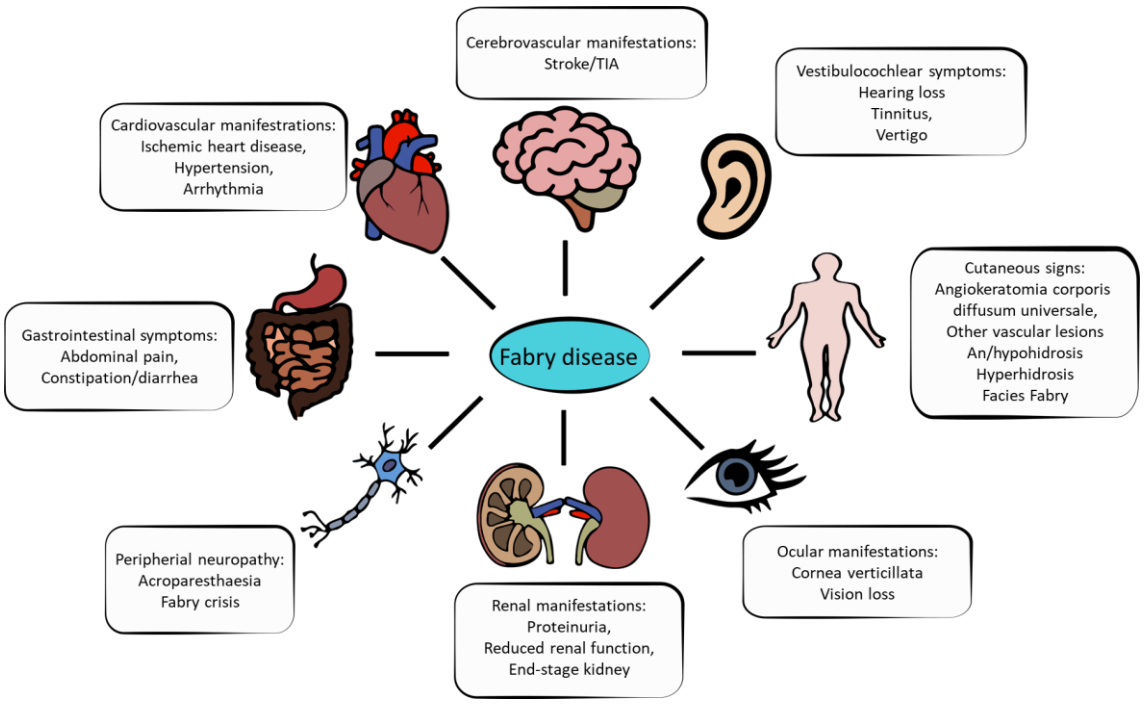

Figure 3. *Overview of the different organ manifestations of Fabry disease.*

Both hemizygous males and heterozygous females can be affected by the disease. Patients with minimal or no AGAL activity exhibit the "classic" phenotype, which features early-onset characteristic symptoms such as angiokeratoma corporis diffusum universale (ACDU), acroparesthesia, and cornea verticillata. From the third decade of life onward, the disease can progress to cause renal, cardio- and cerebrovascular disorders. If left untreated, Gb3 accumulation in various cells leads to irreversible end-organ damage and reduced life expectancy (14). Late-onset variants of the disease, which affect patients between the ages of 30 and 70, usually present milder symptoms and may only affect one or a few organ systems, such as the cardiac or renal variant (12). Heterozygous females may exhibit a range of clinical presentations, from asymptomatic to severe disease, with a lower likelihood of developing the classic phenotype due to residual enzyme activity and X-chromosome inactivation patterns (15).

1.3.3. Diagnosis

The presence of typical organ manifestations and/or a family history may lead to the suspicion of FD. Diagnosis in males can be confirmed by reduced AGAL activity in

plasma, leukocytes, or other cell types. While genetic analysis is not required for diagnosis in males, it is crucial for selecting disease-specific therapies. In females, AGAL enzyme activity may be normal, necessitating genetic analysis to confirm the diagnosis (16).

1.3.4. Angiokeratomas in Fabry disease

The cutaneous hallmark of FD is ACDU (Figure 3.), which is the most prevalent clinical feature of the disease, observed in 66% of male and 36% of female patients (17). ACDU is typically observed in males during childhood and is considered an important sign for early diagnosis. Angiokeratomas are acquired benign vascular lesions that are characterized histologically by dilated subepidermal vessels with overlaying epidermal acanthosis and hyperkeratosis. Angiokeratomas in FD result from the weakening of the vessel wall due to the accumulation of Gb3 in the dermis. Initially presenting as telangiectatic vessels, angiokeratomas can subsequently develop into subepidermal vascular cavernae with occasionally warty hyperkeratosis, manifesting as solitary or clustered red, blue, or black papules or plaques, typically distributed between the navel and upper thighs, also known as the "bathing-suit distribution". Angiokeratomas in FD develop in childhood and typically increase in size and number as the disease progresses (18). Female FD patients typically develop angiokeratomas later and on different localizations e.g. trunk and proximal extremities (17). Macular, flat angiokeratomas in FD have also been described (17). Dermoscopy reveals well-demarcated dark red to blueish-black lacunae corresponding to dilated vascular spaces that may be thrombosed. Hyperkeratosis and acanthosis result in an opalescent whitish veil (19). Differential diagnosis should consider other vascular lesions such as hemangiomas, which share similar dermoscopic features with angiokeratomas. It is important to mention that ACDU is not synonymous with FD. While ACDU is a characteristic feature of FD, it can also occur in a variety of other lysosomal storage diseases (20). Additionally, while angiokeratomas are the most prominent signs of FD, there are subtypes of angiokeratomas that are not associated with FD. Angiokeratomas can be classified into five distinct clinical types based on their location, morphology and etiology, although they share similar histological features: 1.) ACDU, as described earlier, presents in the bathing suit distribution in patients with FD and rarely other lysosomal storage diseases, 2.) angiokeratoma of Mibelli appears on the dorsal surfaces of hands and feet and is often

linked to chilblains, 3.) angiokeratoma of Fordyce can be observed on the scrotum and is associated with increased venous pressure 4.) angiokeratoma circumscriptum naeviforme manifests unilaterally on a lower extremity, and 5.) solitary and multiple angiokeratomas can appear anywhere on the body but are most commonly found on the lower extremities (18).

1.3.5. Other cutaneous signs

In addition to ACDU, other dermatological manifestations of FD include telangiectasias, abnormalities of sweating, lymphedema, and typical pseudoacromegaloid dysmorphia of the face known as "facies Fabry" (18). Sweating abnormalities include an- or hypohidrosis and hyperhidrosis. The etiology of sudomotor dysfunction observed in FD is attributed to nerve damage and the infiltration of storage material into the sweat glands. Hypo- and anhidrosis are established clinical features of FD, affecting a substantial proportion of male patients (93%) and a smaller percentage of female patients (25%). These symptoms can result in heat and exercise intolerance, posing a significant clinical burden to affected individuals. Conversely, hyperhidrosis has recently emerged as a novel indicator of FD, with a higher prevalence among female patients (11.9%) relative to males (6.4%). The recognition of hyperhidrosis as a possible sign of FD, although not as widely reported as hypo- and anhidrosis, has important implications for disease diagnosis and management, particularly in the female patient population (21). Facies Fabry is characterized by prominent supraorbital ridges, periorbital fullness, large bitemporal width, bushy eyebrows, broad nasal base, full lips and prominent chin, which typically occur in the classical, more severe type of the disease (17). Although lymphoedema was included in the initial characterization of FD, it is not considered a distinctive feature of the disease. Accumulating evidence supports a pathogenic connection between FD and the development of edema (25% of males and 17% of females) and lymphoedema (16% of males and 7% of females) in affected individuals (17). The presence of telangiectasias is also a characteristic, but not a specific sign of FD affecting 23% of males and 9% of females (17). While some of the above-described cutaneous signs alone are not conclusive indicators of FD, their consideration in the diagnostic workup may prove useful in the identification of previously undetected cases.

1.3.6. Disease-specific therapy

The timely recognition of FD assumes even greater significance in light of the availability of disease-specific therapies, which can mitigate the progression of disease and improve clinical outcomes. At present, enzyme replacement therapy (ERT) is the mainstay of treatment for FD, with two forms, namely agalsidase-alfa and agalsidase-beta, available for biweekly intravenous administration. A newer therapeutic modality, known as chaperone therapy, involves the use of migalastat to enhance protein folding and stabilize the mutated endogenous AGAL protein. However, the use of migalastat is limited to specific missense mutations. Emerging therapeutic strategies for FD include next-generation ERT, substrate reduction therapy, and gene therapy, which hold promise for more effective and targeted management of the condition in the future (14).

The availability of ERT and chaperone therapy underscores the need for early detection and intervention, as early initiation of disease-specific therapy has been shown to improve clinical outcomes and prevent disease progression. Thus, early recognition of FD is imperative to ensure the timely implementation of disease-specific treatment. The identification of skin manifestations holds significant value in the diagnosis of FD as these visible and early-onset symptoms serve as a conspicuous indication of the underlying disease. Skin manifestations are also a notable cause of morbidity, affecting the individual's self-esteem and quality of life, thus necessitating the application of proper treatment modalities. The extensive heterogeneity of clinical presentations in FD can result in a delayed diagnosis, thus hindering the timely initiation of disease-specific therapy. In this regard, dermatologists play a crucial role in the early recognition and diagnosis of FD, given the high frequency of cutaneous features associated with the condition.

1.4. Imaging of the skin

1.4.1. Clinical photography

Within the field of dermatology, the primary mode of diagnosis predominantly relies on visual observation, a common approach shared by numerous medical specialties. Correspondingly, the utilization of clinical photography has progressively emerged as an essential component of customary medical practice in dermatology. Clinical photography

has gained considerable prominence as a means to record the temporal progression of pathological alterations or the healing trajectory and also serving as a potent communication medium. Moreover, it plays a pivotal role in facilitating precise and prompt diagnosis, while also serving as the most reliable modality for maintaining comprehensive medical records (22).

1.4.2. Dermoscopy

Dermoscopy, a non-invasive *in vivo* technique, is a widely used tool for the assessment of cutaneous lesions. This procedure enables the visualization of skin structures situated within the epidermis, the dermoepidermal junction, and the papillary dermis, which are typically imperceptible to the naked eye. Initially employed in the field of dermato-oncology, dermoscopy has progressively expanded its utility to encompass a broad spectrum of dermatological conditions including infectious skin conditions (entodermoscopy) and inflammatory dermatoses (inflammoscopy) (23, 24). Dermoscopy can unveil subtle findings that might be missed during a routine clinical examination, thereby facilitating accurate diagnoses and appropriate treatment strategies. Besides the utility of clinical photography, dermoscopic images can also be captured through photography or digital recording, facilitating their storage and enabling sequential monitoring to assess for any subsequent alterations.

1.4.3. Multispectral imaging

Multispectral imaging (MSI) refers to a novel non-invasive, *in vivo* technology that captures images using a combination of multiple LED lights with different wavelengths. By using LEDs that emit light at various wavelengths across the visible and non-visible spectrum, the technology can capture images with high spatial resolution and high spectral specificity. The technique can be used to determine the distribution of the endogenous fluorophores of the skin such as keratin, melanin and hemoglobin. Our research group has utilized MSI in the diagnosis of melanoma as well as rare skin diseases including pseudoxanthoma elasticum (25, 26).

1.4.4. Nonlinear microscopy

Nonlinear microscopy (NLM) holds great promise as a label-free imaging technique, predominantly employed in the field of brain research. In the context of skin assessment, NLM techniques, specifically two-photon absorption fluorescence (TPF) and second-

harmonic generation (SHG), offer the potential for high-resolution skin imaging. To achieve the generation of nonlinear optical processes, a high photon density is necessary, which can be attained through femtosecond or picosecond pulse laser systems operating within the near-infrared spectrum (27). Notably, while excitation occurs in the near-infrared wavelength range, the emitted photons fall within the visible light spectrum. TPF enables the visualization of keratins, elastin, and melanin, whereas SHG is employed for the imaging of non-centrosymmetric molecules, such as collagen. Our research group recently applied these two modalities for the *ex vivo* assessment of basal cell carcinoma, pseudoxanthoma elasticum and Ehlers–Danlos syndrome (28-30). Several other investigations have been conducted on various skin conditions, leading to a comprehensive understanding of the nonlinear microscopic characteristics exhibited by inflammatory skin conditions such as atopic dermatitis or psoriasis (31).

2. OBJECTIVES

In overview, we aimed to apply multimodal imaging, namely MSI and NLM in case of rare, inherited disorders presented with disordered keratinization or vascular lesions.

- Our first aim was to investigate the use of MSI in keratinization disorders with a focus on a rare KPI caused by a *KRT1* gene mutation. We evaluated MSI in detecting and visualizing optical changes in the skin in the case of EI.
- We aimed to utilize *ex vivo* NLM modalities with a particular focus on the visualization of alterations brought on by hyperkeratosis.
- We assessed the utility of MSI for evaluating angiokeratomas in FD patients. Our aim was to capture autofluorescence and diffuse reflectance images of angiokeratomas and compare the images to dermoscopy to determine whether MSI provides additional information.
- We explored the application of *ex vivo* NLM for distinguishing angiokeratomas from other vascular lesions such as hemangiomas.
- We characterized the clinical and morphologic features of angiokeratomas in patients with FD. Our objective was to examine the distribution, appearance, and variability of angiokeratomas in FD. This involved conducting a thorough dermatological examination, evaluating dermoscopic images, and describing the specific structures observed in angiokeratomas.
- We investigated the diagnostic challenges and heterogeneity of dermatological manifestations in FD. Our aim was to explore the clinical heterogeneity of FD in our patient cohort and its impact on the diagnosis of the condition. We analyzed the distribution and appearance of angiokeratoms, to understand the diagnostic challenges faced by healthcare professionals. Additionally, we evaluated other cutaneous signs of FD, that can contribute to the early diagnosis of the condition.

3. METHODS

3.1. Visualization of keratin with multispectral imaging and nonlinear microscopy in a rare keratinopathic ichthyosis

3.1.1. Patient and genetical analysis

We conducted the assessment of the skin lesions in a 3-year-old male patient with EI using *in vivo* MSI and *ex vivo* NLM to specifically investigate and visualize the changes associated with hyperkeratosis. For the confirmation of the diagnosis, genetic analysis was carried out. The genomic DNA was extracted from peripheral blood leukocytes obtained from the patient as well as his parents. The amplification of exons and adjacent intron regions was carried out using predetermined *KRT1*-specific primers that were tagged with M13 tail sequences. This amplification process was conducted using the VariantSEQr PCR sequencing system (Applied Biosystems, Foster City, CA, USA).

3.1.2. Multispectral imaging

For *in vivo* MSI imaging, an experimental setup described in previous studies (32, 33) was employed, utilizing an LED-based device. A series of autofluorescence images were captured under continuous excitation of a 405 nm LED. Furthermore, diffuse reflectance images were obtained using 526 nm illumination. To ensure consistent illumination and a fixed distance of 60 mm between the camera and the uniformly lit skin, a cylindrical light-shielding wall was utilized, which housed four battery-powered violet and green LEDs. A long pass filter (>515 nm) was positioned in front of a color CMOS 5-megapixel IDS camera (MT9P006STC, IDS uEye UI3581LE-C-HQ, Obersulm, Germany) to prevent the detection of 405 nm LED emissions. The skin of the patient was evaluated at two distinct locations in order to compare the inherent autofluorescence of unaffected skin with the changes induced by hyperkeratosis. A healthy child of matching age and gender was also assessed as a control using the same methodology. In all images, areas of affected and unaffected skin were manually selected as regions of interest (ROI). The mean autofluorescence and diffuse reflectance intensity values within the selected ROIs were analyzed using ImageJ v1.52a software (NIH, Bethesda, MD, USA). Autofluorescence and diffuse reflectance intensity values were calculated based on the Integrated Optical Density (IOD) measurement functionality of the ImageJ software. IOD values are given in an arbitrary unit.

3.1.3. Nonlinear microscopy and conventional histology

Skin biopsies were performed using a 4 mm punch biopsy tool. Specifically, two samples were obtained from the plantar region of the patient with keratoderma for NLM imaging. One of the biopsy specimens was immediately transferred in phosphate-buffered saline and positioned on slides to capture z-stack images using NLM. The second biopsy sample was fixed in formalin, embedded in paraffin, and sliced into 20 μm thick sections. Following deparaffinization, the unstained sections were covered with coverslips to enable the acquisition of vertical NLM images. For histopathologic analysis, hematoxylin and eosin (H&E) stained sections were prepared using standard techniques. To serve as a control, an equivalent set of samples from an unaffected individual underwent identical treatment and processing. For NLM imaging, a sub-ps Ti:Sapphire laser (FemtoRose 300 TUN LC, R&D Ultrafast Lasers Ltd., Budapest, Hungary) with a repetition rate of approximately 20 MHz was utilized. The imaging system employed was a commercial Axio Examiner LSM 7 MP laser scanning 2P microscope, equipped with a 20×, 1.0 NA water immersion objective (W-Plan-APOCHROMAT, Carl Zeiss Microscopy GmbH, Jena, Germany). The pump laser was set to a central wavelength of 800 nm, with a bandwidth of less than 2 nm. A 405/20 nm bandpass filter was employed to collect the SHG signal, while a 590/45 nm (orange) bandpass filter was used for the collection of the TPF signal prior to detection by non-descanned detectors. Two-channel, 16-bit images were acquired from individual imaging areas measuring 420 × 420 μm², with a pixel dwell time of 12 μs. Mosaic images of vertical skin sections were captured, and the acquired TPF and SHG images were merged and assembled into two-channel images using ImageJ v1.46 software (NIH, Bethesda, MD, USA). Z-stacks of the skin biopsy samples were obtained with a 5 μm step size between horizontal images using Zeiss Zen software v3.0 (Carl Zeiss AG, Germany). Three-dimensional images were generated from these 2D images along the z-axis using ImageJ software.

3.2. Assessment of angiokeratomas in Fabry disease

3.2.1. Patients and diagnosis

In this study, we presented findings from a cohort of 26 patients belonging to 16 families who were referred to our hospital diagnosed with FD. The diagnosis of FD was established based on reduced AGAL activity, and genomic DNA sequencing. A comprehensive dermatological examination, including dermoscopic evaluation and

photographic documentation, was conducted. For two patients (one male and one female), the diagnosis of angiokeratoma was further confirmed through histopathological analysis. Data related to the extracutaneous manifestations of FD were retrospectively collected from clinical records. Prior to their inclusion in the study, informed consent was obtained from all participating patients.

3.2.2. Dermoscopy

We examined dermoscopic images of randomly selected lesions using the Heine Delta 20 dermatoscope (Heine Optotechnik GmbH, Herrsching, Germany). Our evaluation focused on identifying specific features, including red, blue, or black lacunae, as well as the presence of a whitish veil. Additionally, we assessed the structure of the vasculature within the lesions. We employed both descriptive and commonly used metaphorical dermoscopic terminology (19, 34).

3.2.3. Multispectral imaging

We assessed seven FD patients presenting angiokeratomas with LED-based MSI. The same setup was used as described in section 3.1.2. In addition to autofluorescence images under 405 nm illumination and diffuse reflectance images under 526 nm illumination, we recorded and evaluated diffuse reflectance images under 663 nm and 964 nm illumination.

3.2.4. Nonlinear microscopy and conventional histology

For NLM investigations, deparaffinized and unstained sections obtained from the angiokeratoma biopsies were prepared. NLM imaging was conducted with the same setup as described in section 3.1.4., with the following modifications. To collect the SHG (collagen) signal, a 405/20 nm bandpass filter was utilized as described above, while a 525/50 nm (green) bandpass filter was employed to collect the TPF signal. The selection of the green channel was based on preliminary measurements conducted on blood samples. The acquired TPF and SHG images were merged and combined into two-channel images using ImageJ v1.46 software (NIH, Bethesda, MD, USA). For histopathologic analysis, H&E stained sections were prepared using standard techniques.

3.2.5. Ethical statement

All procedures performed in studies involving human participants were in accordance with the ethical standards of the institutional research committee (Semmelweis University Regional and Institutional Committee of Science and Research Ethics, Budapest,

Hungary, SE TUKEB no. 193/2017 and 228/2018) with the 1964 Declaration of Helsinki and its later amendments or comparable ethical standards.

4. RESULTS

4.1. Case presentation of a rare keratinopathic ichthyosis and assessment with multispectral imaging and nonlinear microscopy

4.1.1. Case presentation

We present the case of a 3-year-old male patient who displayed brownish, red, scaly patches in intertriginous and umbilical regions, concomitant with palmoplantar hyperkeratosis (Figure 4.). Shortly after birth, the infant presented with blistering and erosions, accompanied by pronounced scaling on the scalp, flexural and intertriginous areas, as well as the palmoplantar regions. The severity of the observed symptoms exhibited temporal fluctuations (Figure 5.), with intermittent episodes of exacerbated epidermolysis, fissures, and onychodystrophy. Remarkably, the parents did not possess any pertinent medical history associated with cutaneous disorders.

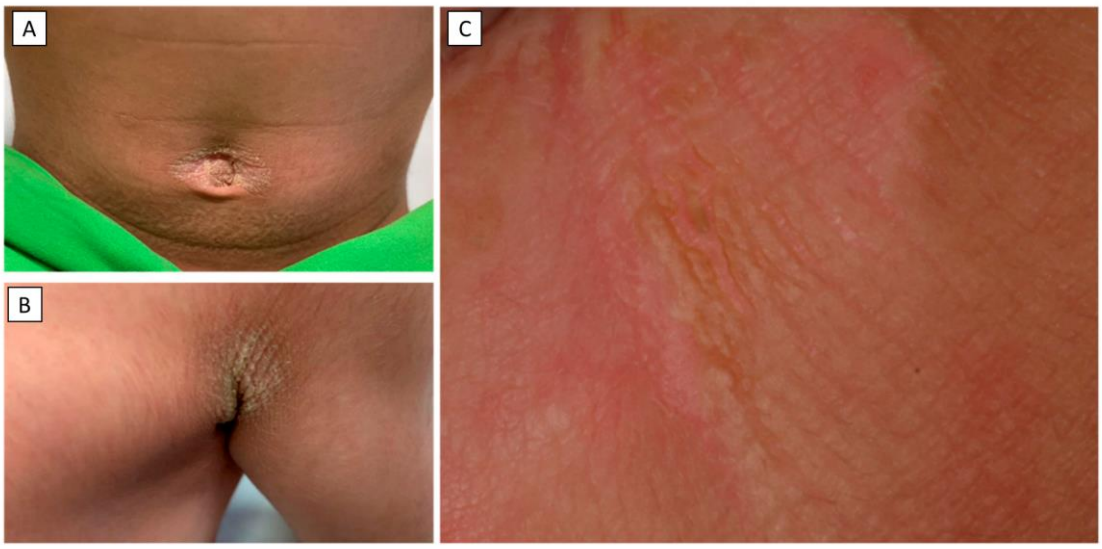

Figure 4. *Skin signs of the patient with epidermolytic ichthyosis. Hyperkeratotic plaques in the umbilical (A) and axillary (B) regions of the affected individual. In addition, a notable hyperkeratotic plaque with mild epidermolysis, fissures, and lichenification was observed in the gluteal region (C).*

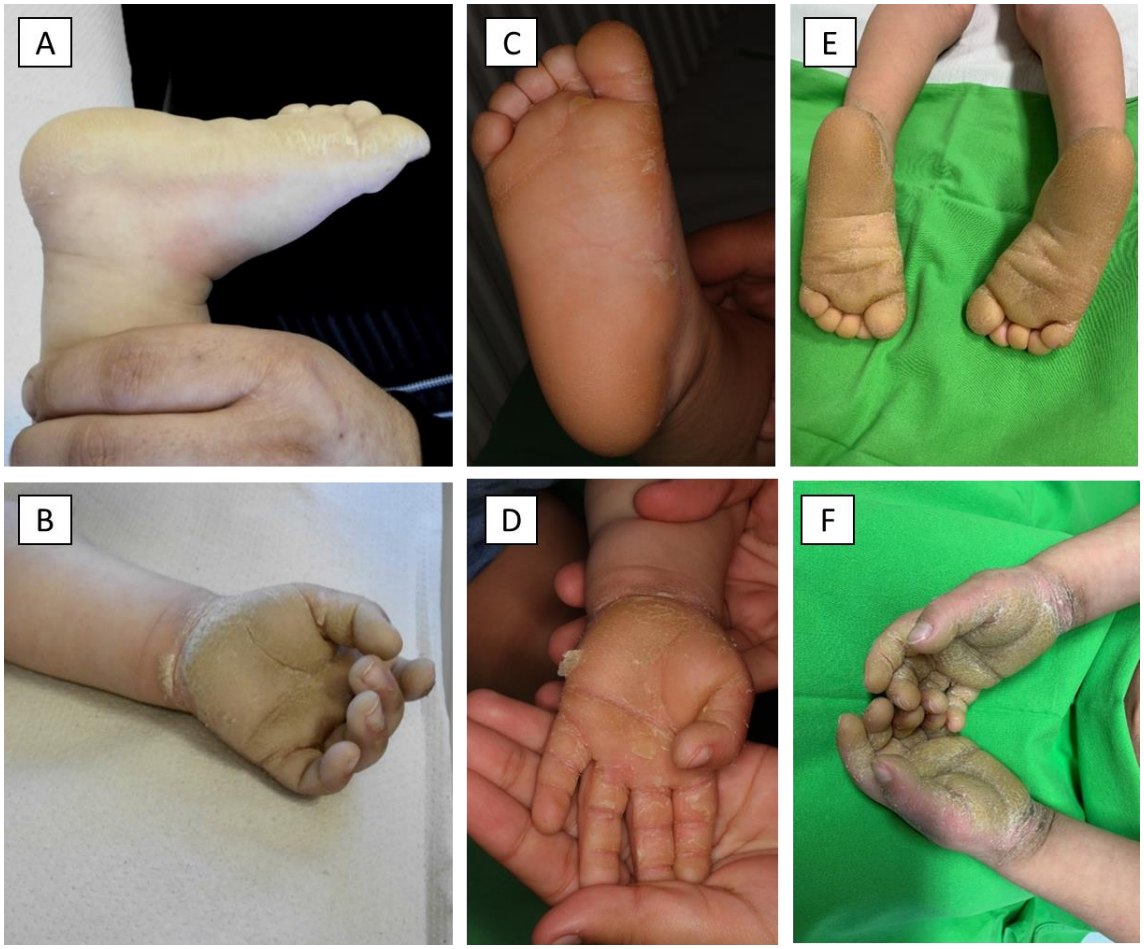

Figure 5. *Diffuse palmoplantar keratoderma of the patient at the age of 6 months (A, B), 1 year (C, D), and 3 years (E, F). The presence of hyperkeratosis extending beyond the boundaries of the palms and soles can be noted. In our specific case, the severity of palmoplantar keratoderma (PPK) demonstrated fluctuations over time.*

Genetic analysis of the *KRT1* gene in the proband revealed the presence of a heterozygous missense mutation c.1436T>C. This mutation, designated as p.Ile479Thr, induces an amino acid substitution from isoleucine to threonine within the highly conserved 2B domain of keratin 1 (Figure 6.). Notably, the genetic analysis conducted on the parents did not reveal the presence of this pathogenic variant. Furthermore, an in-frame deletion variant encompassing 21 base pairs within exon 9 of the *KRT1* gene (p.Gly553-Tyr559del) was identified in both the proband and the proband's mother (35).

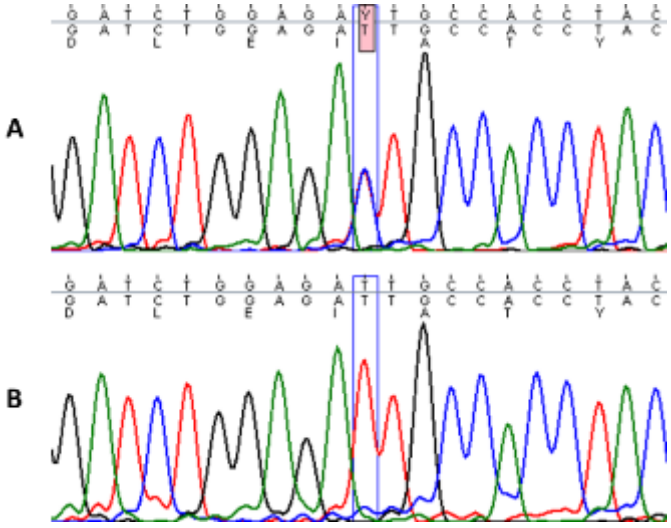

Figure 6. *Sequence analysis of the affected patient with heterozygous mutation c.1436T>C in KRT1 gene (A) and homozygous wild-type sequence in a healthy individual (B).*

4.1.2. Multispectral imaging

In comparison to the unaffected skin region on the patient's arm and both evaluated skin sites of the healthy control, the thickened palmar hyperkeratosis exhibited significant autofluorescence upon excitation at 405 nm illumination (Figure 7.). Moreover, a lower level of diffuse reflectance signal was observed when the area was illuminated with 526 nm. Through quantitative analyses, it was determined that the palmar hyperkeratosis displayed a notably higher average autofluorescence intensity compared to the clear palmar skin and unaffected skin region of the patient (162.35 vs. 51.14 vs. 20.46). In contrast, the average autofluorescence intensity in the unaffected region of the patient and the healthy control demonstrated a slightly lower value (20.46 vs. 35.97). Concerning the palmar skin, the mean intensity values of the diffuse reflectance images under 526nm excitation were higher in both the patient and control groups (45.83 and 48.12, respectively) when compared to the forearm skin of the patient and control (35.01 and 36.01, respectively). Notably, there was no substantial difference observed in the mean intensity values of the diffuse reflectance imaging between the patient and the healthy control groups (Table 1.).

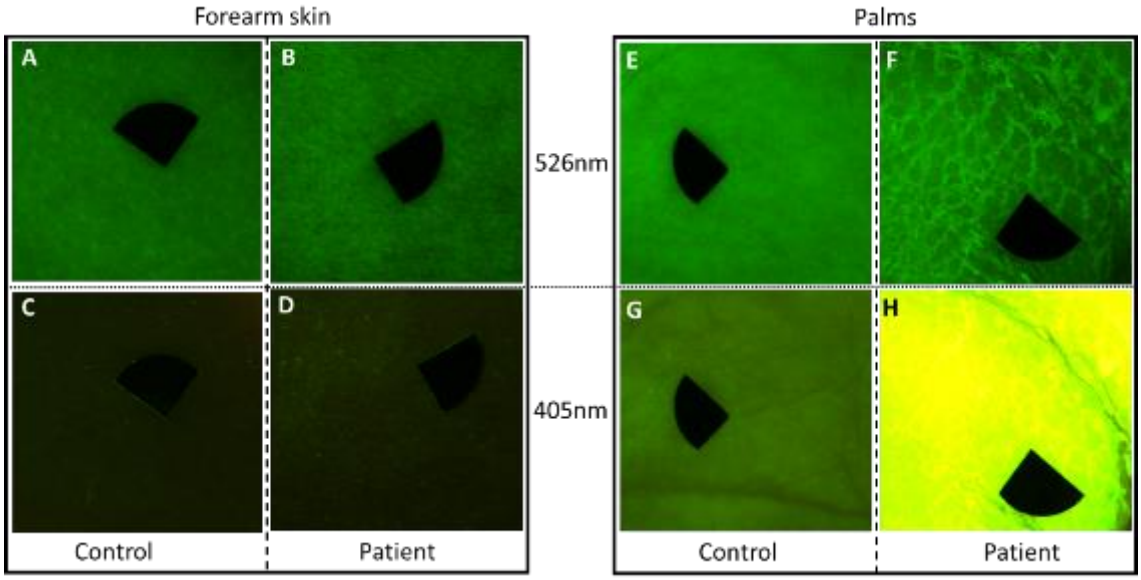

Figure 7. *Diffuse reflectance images were obtained from the patient and a healthy age-matched individual using 526 nm illumination (A, B, E, F), while autofluorescence images were captured under 405 nm LED excitation (C, D, G, H). Images A to D represent the unaffected skin region on the patient's forearm and the corresponding area on the healthy individual, showcasing the inherent autofluorescence of the skin. Images E to H depict the palmar skin. In image F, the edges of the thickened scales were delineated using 526 nm illumination on the patient. Notably, image H shows that the thick hyperkeratotic layer on the palm exhibited a strong autofluorescence signal upon excitation at 405 nm. Image size: 2 × 2 cm². The black markers in the images do not indicate areas of interest but serve for image alignment. The pixel size is 180 pixels/cm.*

Table 1. Mean diffuse reflectance and autofluorescence intensity values. IOD: integrated optical density, au: arbitrary unit

Image	Area (pixel^2)	IOD (au)	Mean intensity value
A	93526	3367091	36.01
B	182298	6382257	35.01
C	81545	2933298	35.97
D	113030	2312653	20.46
E	113220	5447741	48.12
F	178957	8201498	45.83
G	101910	5211317	51.14
H	116840	18968786	162.35

4.1.3. Nonlinear microscopy

The visualization of the papillary dermis in the fresh frozen plantar keratoderma sample was hindered due to the presence of thick hyperkeratosis and strong autofluorescence of keratin. These factors caused significant scattering and resulted in a reduced depth of penetration (Figure 8.). The maximum depth reached within the skin was measured at 115 µm for the plantar keratoderma sample and 230 µm for the control sample (Figure 8.).

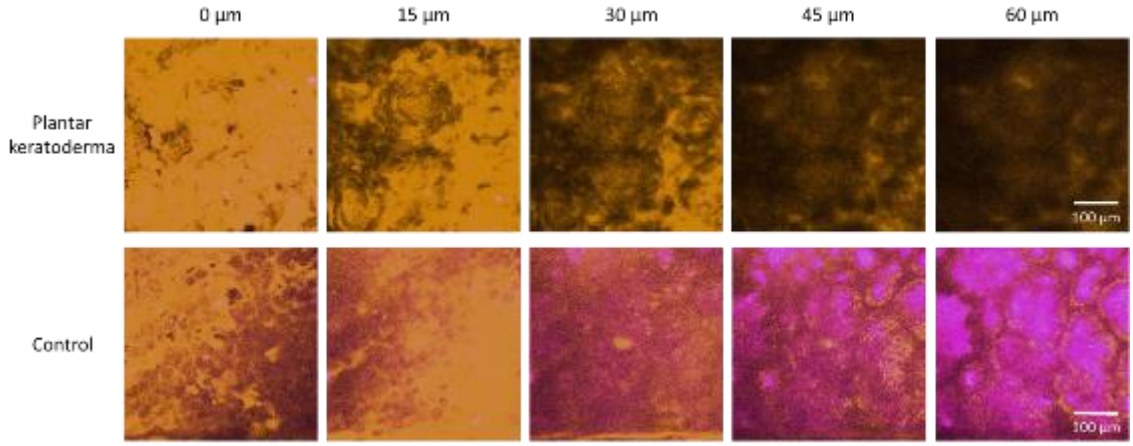

Figure 8. *Horizontal optical slicing of skin biopsies from the epidermis to the dermis was performed using nonlinear microscopy. The upper panel represents a sample from a patient with plantar keratoderma, while the lower panel shows a biopsy from a healthy control. Representative images were acquired at five different vertical positions along the z-axis, with a separation of 15 µm between each position. The skin biopsies were horizontally positioned on the microscopy slides for imaging. Orange color (590/45 nm bandpass emission filter) and magenta color (405/20 nm bandpass filter) indicate two-photon absorption fluorescence (TPF) and second-harmonic generation (SHG) signals, respectively, in the imaging plane. Scale bar: 100 µm. Pixel size: 0.8476 pixels/µm.*

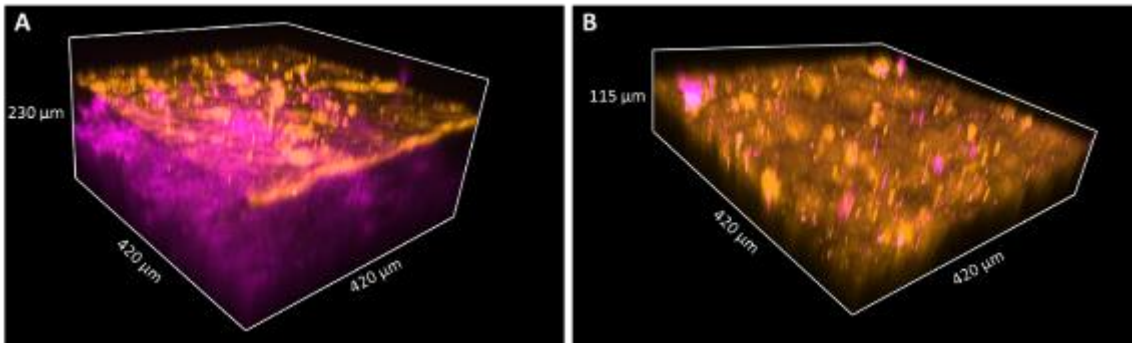

Figure 9. *Three-dimensional (3D) images of keratin and collagen were obtained using two-photon fluorescence (TPF) and second-harmonic generation (SHG) imaging techniques in skin biopsies. Image (A) corresponds to a healthy subject, while image (B) represents a case of palmoplantar keratoderma. Notably, when the epidermis expands, the penetration depth of the pump laser decreases significantly, resulting in the inability to reach the papillary dermis in the case of keratoderma. The size of the images is as follows: 420 × 420 µm.*

For further investigations, formalin-fixed sections that were previously embedded in paraffin were deparaffinized and subjected to imaging with TPF and SHG. For a more conventional representation, two-dimensional vertical cross-section mosaic images were acquired. Notably, the SHG visualization of collagen allowed for the observation of the papillary dermis at the base of the plantar keratoderma sample (Figure 10.). In the TPF channel, the cellular portion of the epidermis was distinguishable between the dermal papillae. However, as the observation moved towards the upper layers, the cellular structures were no longer discernible and were replaced by lamellae in the TPF channel, representing cornified keratinocytes and protein aggregates. These histological changes were consistent with the findings of H&E stained sections (Figure 11.). In contrast, the control skin sample's NLM image allowed for clear visualization of the thin epidermal layer and the collagen network present in the dermis and subcutis.

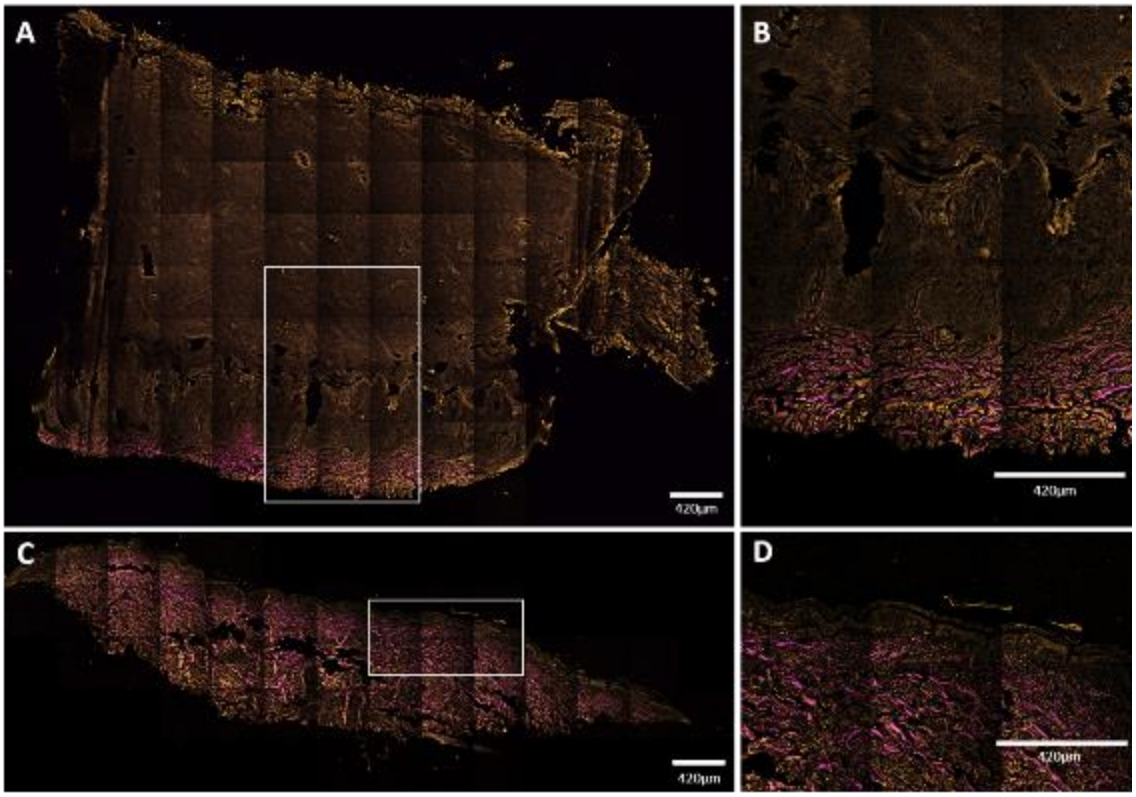

Figure 10. *Mosaic images of vertical skin sections were captured using nonlinear microscopy (NLM). In images (A) and (B), the sections correspond to a patient with plantar keratoderma, while images (C) and (D) represent a healthy control. Keratin was visualized with a two-photon fluorescence (TPF) signal in the orange channel, while collagen exhibited a second-harmonic generation (SHG) signal, indicated by the magenta color. In images (A) and (B), the dermal papillae appeared in magenta, followed by the basal keratinocyte layer shown in orange. Moving upwards, wider cellular layers of the epidermis were observed, accompanied by an increased presence of lamellar structures composed of cornified keratinocytes. The total thickness of the epidermis measured approximately 3000 µm (range: 3079–3373 µm). In images (C) and (D), the structure and proportion of the epidermis appeared as expected in healthy subjects. The thickness of the epidermis averaged around 100 µm (range: 96–146 µm). Scale bar: 420 µm. Pixel size: 0.1571 pixels/µm (A, C); 0.4012 pixels/µm (B, D).*

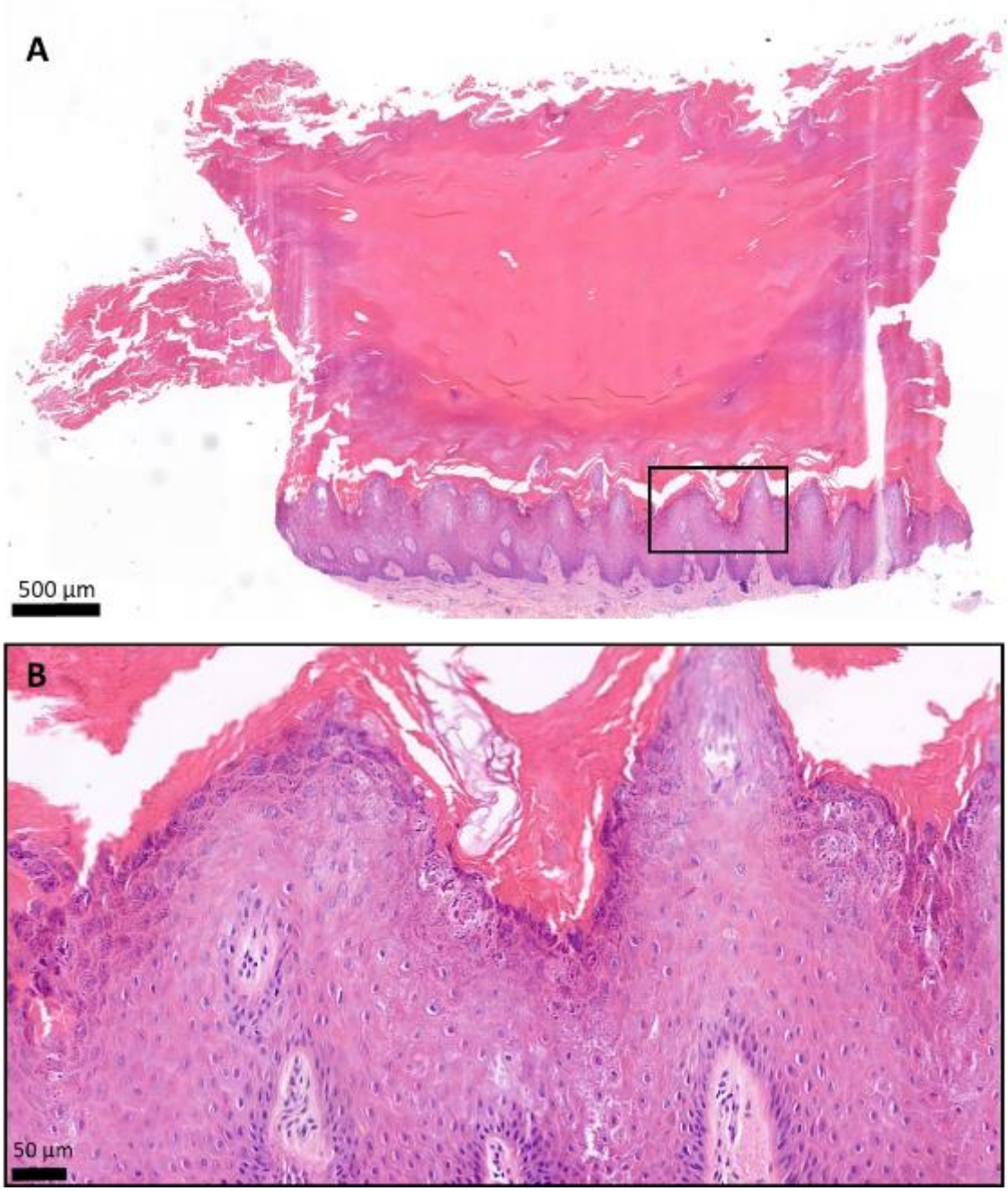

Figure 11. *The histological analysis of the patient's plantar keratoderma using hematoxylin and eosin (H&E) staining revealed a characteristic structure consistent with acral localization. In image (A), the surface of the skin biopsy specimen was covered by a thick layer of hyperkeratotic and orthokeratotic horny tissue. In image (B), it was observed that the epidermis exhibited significant acanthosis (epidermal thickening) and mild papillomatous changes. The stratum granulosum, a layer of the epidermis, appeared widened. The keratohyaline granules within the keratinocytes exhibited varied shapes and sizes and demonstrated perinuclear vacuolization. The basal membrane of the*

epidermis remained intact. (A) 2.8× magnification; scale bar: 500 µm; pixel size: 0.184 pixels/µm. (B) 19.9× magnification; scale bar: 50 µm; pixel size: 1.12 pixels/µm.

4.2. Assessment of angiokeratomas and other cutaneous signs in Fabry Disease

4.2.1. Patient cohort, extracutaneous manifestations

The study population comprised 12 males and 14 females, ranging in age from 5 to 70 years, with a mean age of 38±20.8 years. The age at which FD was diagnosed ranged from 4 to 60 years, with a mean age of 32.8±19.4 years (Table 2.). Among our patients, 16 individuals were diagnosed based on a family member's affected status, while in the remaining portion of our patient group, characteristic organ symptoms led to the clinical suspicion of FD, most commonly in the form of ACDU in 4 patients. Following confirmation of the diagnosis, disease-specific treatment was promptly initiated for the majority of patients (Table 2.). Patients who are currently not receiving the specific therapy exhibit no initial signs of organ involvement and undergo regular screenings for such manifestations.

Table 2. Clinical details of Fabry disease patients in our cohort

	Total (n=26)	Females (n=14)	Males (n=12)
Mean age (years)	38.0±20.9	42.1±19.9	31.1±21.7
Mean age at diagnosis (years)	32.8±19.4	37.07±17.4	27.75±21.1
Mean age at the initiation of therapy (years)	36.1±18.3	43±15.1	29.70±19.4
Therapy			
Agalsidase-α	10 (38%)	5 (19%)	5 (19%)
Agalsidase-β	8 (31%)	4 (15.5%)	4 (15.5%)
Migalastat	1 (4%)	0 (0%)	1 (4%)
None	7 (27%)	5 (19%)	2 (8%)

Among the patients included in the study, cornea verticillata, a usually asymptomatic condition affecting the corneal epithelium, was the most prevalent extracutaneous manifestation, observed in 18 individuals each. This was followed by cardiac

involvement and acroparesthesia, a sensation of tingling, burning, pain or numbness in the extremities. Renal involvement was observed in ten patients, ranging from mild proteinuria to severe organ failure requiring dialysis in two male patients. Pulmonary manifestations were infrequent and mostly subclinical, resulting in restrictive or mixed restrictive-obstructive ventilatory impairment (Table 3.).

Table 3. Extracutaneous manifestations in our patient group

	Total (n=26)	Females (n=14)	Males (n=12)
Cardiovascular involvement			
Cardiac involvement	17	9	8
Arrhythmia	9	5	4
Left ventricular hypertrophy	14	7	7
Ischemic heart disease	2	1	1
Sudden cardiac arrest	1	0	1
Hypertension	10	6	4
Cerebrovascular involvement			
Headaches	4	1	3
Tinnitus	1	0	1
Vertigo	1	1	0
Stroke	4	3	1
Hearing impairment	5	2	3
Renal involvement	11	6	5
Acroparesthaesia	16	6	10
Ophthalmologic signs			
Cornea verticillata	18	9	9
Other nonspecific signs	14	8	6
Gastrointestinal involvement	11	4	7
Pulmonary involvement	4	3	1

4.2.2. Clinical presentation of angiokeratomas

Angiokeratomas were detected in the majority of our patient cohort, comprising 13 female and 11 male patients (Figure 12.). However, during a comprehensive clinical examination, it was observed that one young male and one young female patient did not exhibit any angiokeratomas.

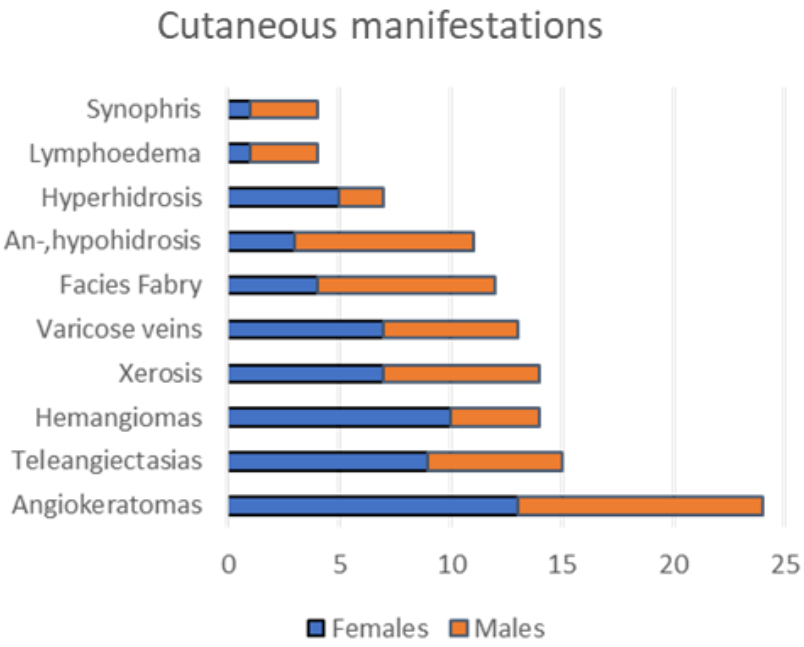

Figure 12. *Cutaneous manifestations of Fabry disease in our patient cohort (n=26). The most common skin findings were angiokeratomas, with other vascular lesions such as telangiectasias and hemangiomas. It is noteworthy that half of our patients had varicose veins, even younger patients, and we also identified synophrys in four individuals.*

The typical form of ACDU in the bathing-suit distribution was observed in eight males and two females, with angiokeratomas primarily localized between the navel and the knees. In more severe cases, ACDU also extended toward the upper extremities. Within our patient cohort, a wide range of angiokeratoma phenotypes could be observed. Typically, male patients presented with extensive, hyperkeratotic, and wart-like angiokeratomas (Figure 13. A-C), while other patients displayed dark red to purple macules corresponding to vessel ectasia without overlying hyperkeratosis (Figure 13. D-G).

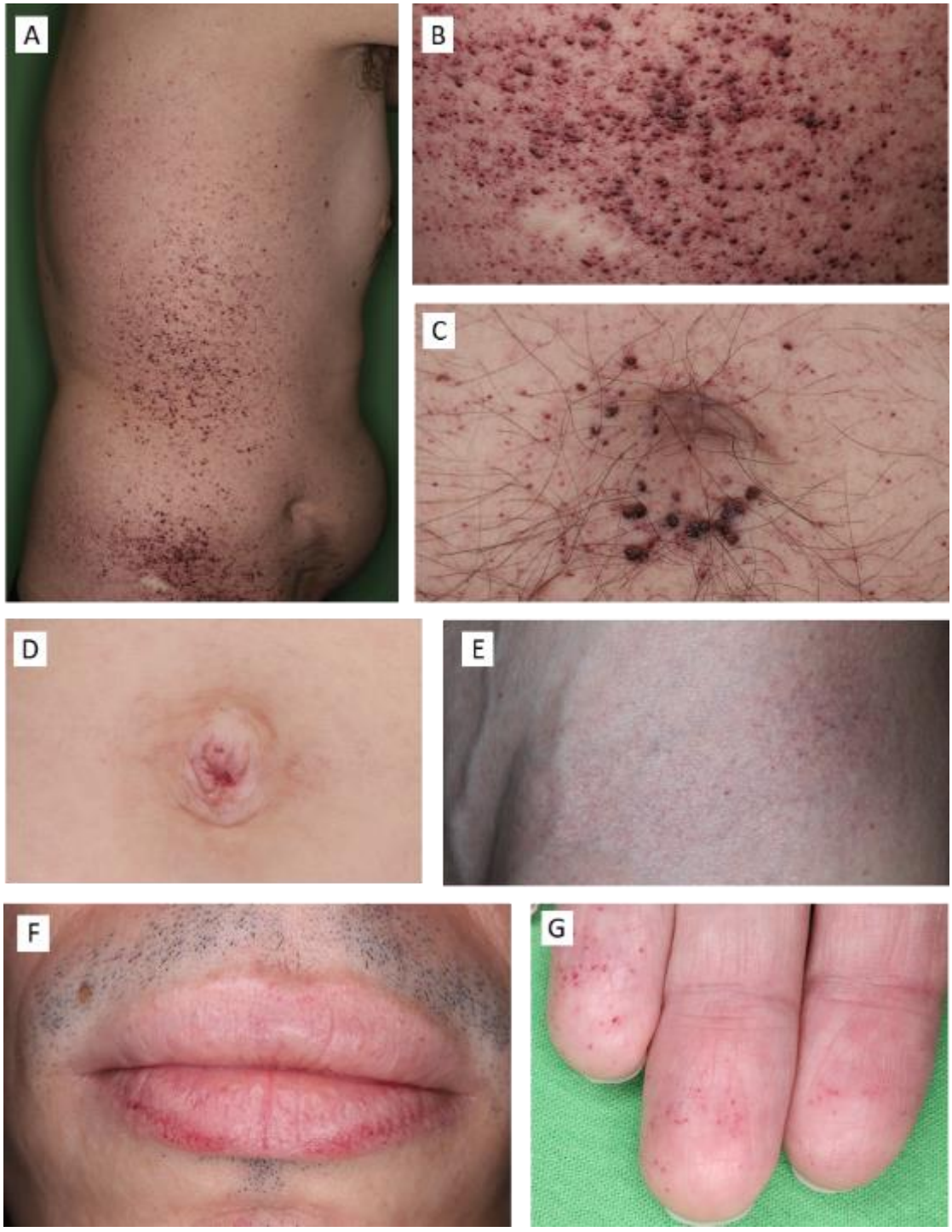

Figure 13. *Angiokeratoma corporis diffusum universale in Fabry disease in male patients. A-C: warty, papular angiokeratomas on the trunk (A), inguinal region (B) and umbilical region (C). D-G: incipient, macular angiokeratomas in the umbilical region of a young male patient (D), inguinal region (E), on the lips (F) and on the fingertips (G).*

We referred to the latter phenotype as incipient or macular angiokeratomas. Women typically presented a smaller number of solitary, papular angiokeratomas without prominent hyperkeratosis, which could be easily confused with senile angiomas (Figure 14.).

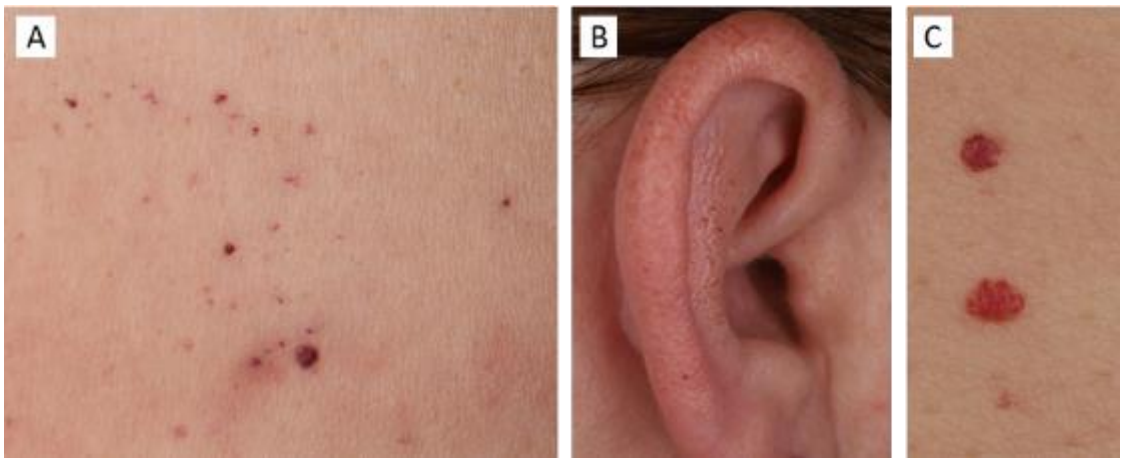

Figure 14. *Angiokeratoma corporis diffusum universale with warty angiokeratomas on the lower abdomen of a female patient (A), macular angiokeratomas on the helix and anthelix of a female patient (B), solitary angiokeratomas on the chest of a female patient (C). Note that solitary angiokeratomas in female patients can be mistaken for hemangiomas.*

It is important to note that although wart-like angiokeratomas are easily identifiable, incipient and solitary lesions can be missed without the aid of dermoscopic examination in some cases. Overall, the most commonly affected sites for angiokeratomas in our patient cohort were the chest, followed by the abdomen and umbilical region (Figure 15.).

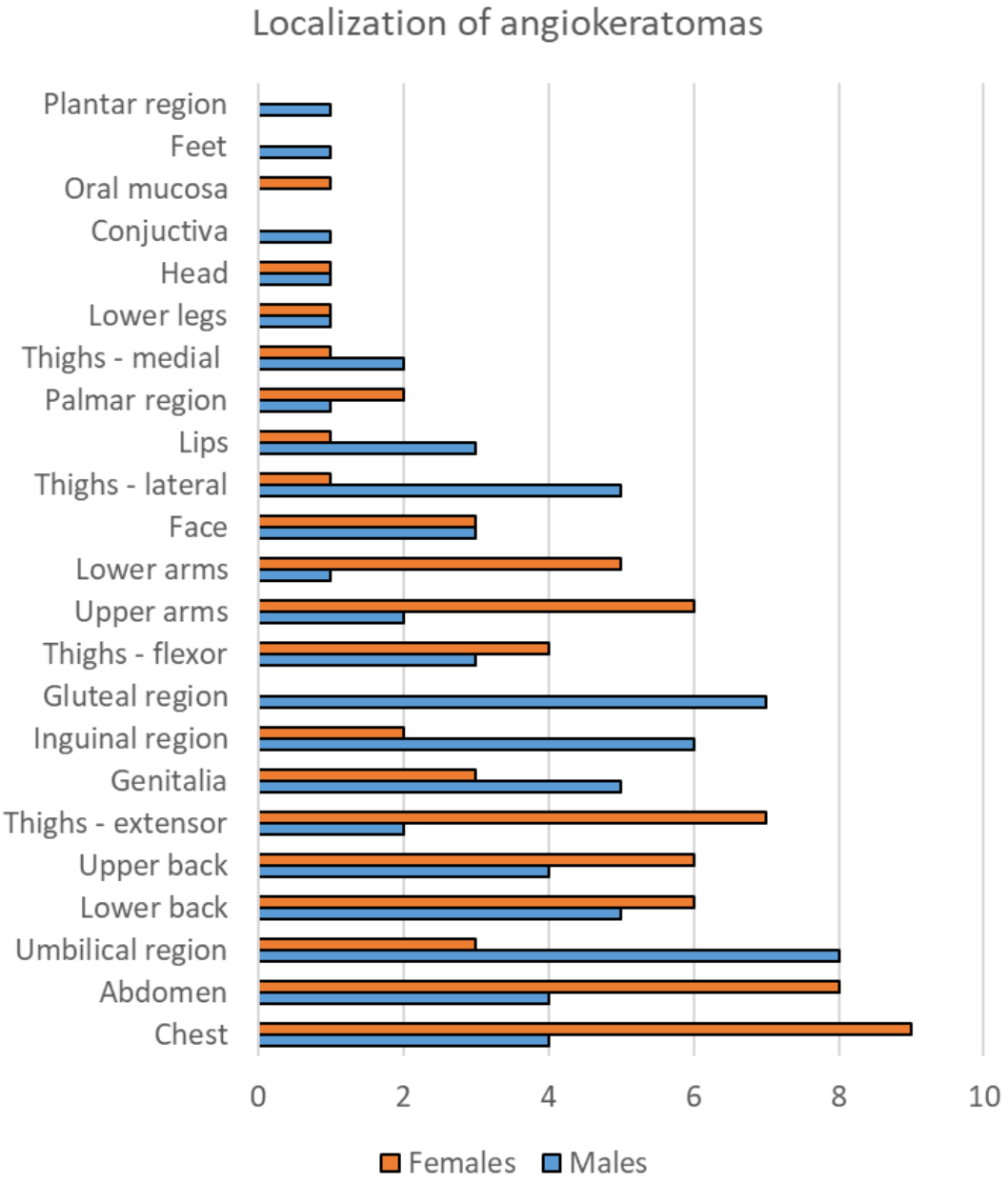

Figure 15. *Frequency of angiokeratomas on different skin sites in males and females in our patient cohort. The chest was the most frequent location for angiokeratomas, with a higher prevalence among females. Among males, the umbilical, gluteal, and inguinal regions were the most common sites, which aligns with the bathing suit distribution.*

Skin areas associated with the typical bathing suit distribution, such as the umbilical region, gluteal region, thighs, and genitalia, were more frequently affected in males, while the chest, upper extremities, and upper back were more commonly involved in female patients. We also observed angiokeratomas in acral locations, including the palmoplantar

region, ears, and lips (Figure 13. F, G, Figure 14. B, Figure 15.). Mucosal involvement was rare, and no angiokeratomas were found on the dorsal surface of the hands within our patient group.

In this study, we made a distinction between the typical and atypical distribution of angiokeratomas, with the typical distribution referring to the bathing suit distribution. Within our patient group, males were more likely to exhibit angiokeratomas in the typical bathing suit pattern, while a larger proportion of females displayed angiokeratomas on atypical skin sites such as the upper trunk and arms (Figure 16.).

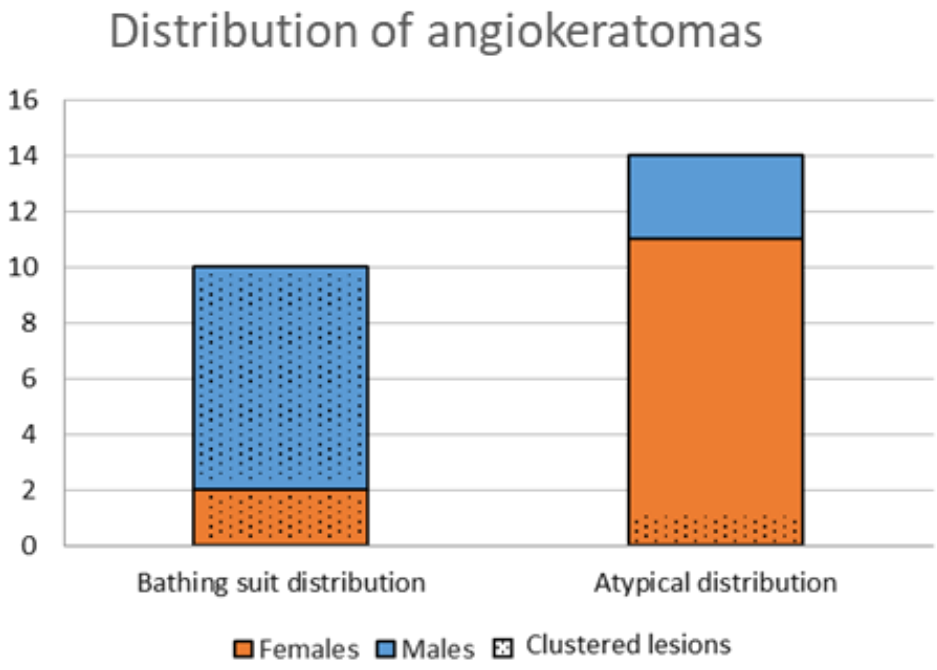

Figure 16. *Distribution of angiokeratomas in males and females. The columns with dots indicate patients who had grouped angiokeratomas, while the solid-colored columns represent patients with solitary lesions. Note that all patients who presented angiokeratomas in the bathing suit distribution had grouped lesions, while most patients presenting angiokeratomas on atypical skin sites e.g. chest, and upper extremities almost exclusively presented solitary lesions.*

In cases of typical distribution, angiokeratomas appeared in clusters, whereas in instances of atypical distribution, solitary lesions were more characteristic. Among patients with

atypical distribution, the majority, consisting of three males and eight females, had only a small number (less than 5) of angiokeratomas. Only three females in the atypical distribution group presented with a higher number of angiokeratomas. This included two middle-aged women who had several solitary papular lesions on the trunk and upper extremities, as well as one young female patient who exhibited clustered incipient angiokeratomas exclusively on the upper arms. These findings indicate that only 10 of our patients displayed the "classic" ACDU phenotype, while other cases demonstrated either a small number of lesions or atypical features in terms of distribution and clinical appearance and were not conspicuous upon clinical examination.

4.2.3. Other cutaneous manifestations

In regards to other cutaneous manifestations in our patient group, 11 patients exhibited an- or hypohidrosis (eight males and three females), and an additional seven patients presented with hyperhidrosis (two males and five females) (Figure 12.). Notably, reduced sweating was frequently accompanied by dry skin. Furthermore, a majority of our patients displayed various vascular lesions, including telangiectasias and cherry angiomas. Interestingly, almost half of the patients exhibited pseudoacromegaloid features to varying degrees. Varicose veins were prevalent in our patient population and could even be observed in young patients (Figure 17. A-B). Lymphoedema was also identified in five adult patients (Figure 17. C). Additionally, synophrys was observed in four young patients, both males and females (Figure 17. D-E). Importantly, patients with a low number of angiokeratomas or even those devoid of any angiokeratomas exhibited other cutaneous signs that hold considerable diagnostic value.

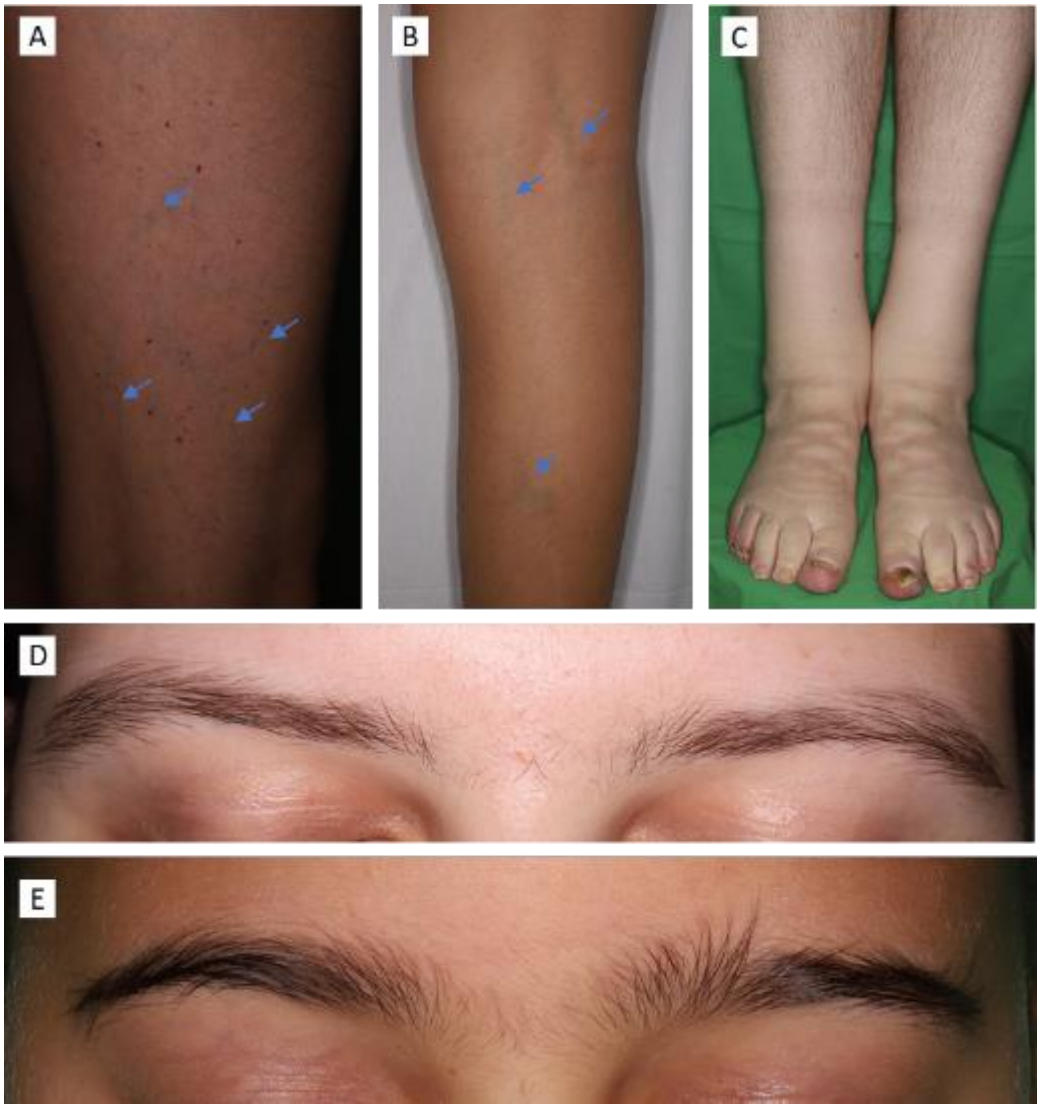

Figure 17. *Other cutaneous signs of Fabry disease. A-B: Varicose veins (blue arrows) on two young male patients. The young male patient in panel A also presented with several angiokeratomas. C: Lymphoedema in a middle-aged male patient. D-E: Synophrys in the case of a young female and male patient.*

4.2.4. Dermoscopic features of angiokeratomas

A total of 135 dermoscopic images of angiokeratomas were analyzed, and we evaluated the vascular architecture, coloration, and the presence of a whitish veil. Our classification of vascular structures encompassed four main types: glomerular, lacunar, dot-like, and linear-irregular (Figure 18.). Glomerular vessels were identified in 30% of the cases, while approximately two-thirds of the cases exhibited lacunae, and more than half of the cases manifested as dot-like vessels. Notably, the co-occurrence of lacunae and dot-like

vessels was a prevalent observation, with 44% of the examined cases displaying both features. The presence of a whitish veil, corresponding to overlaying hyperkeratosis, was detected in only 25% of the cases examined. Furthermore, structureless milky-red areas were discernible in 26% of the cases, where neither vascular structures nor the hyperkeratotic whitish veil could be observed. The color of the lesions was dark purple or red in the majority of cases, accounting for two-thirds of the observations. Bright red vasculature was observed in 18% of cases, while in 16% of cases, lesions exhibited both colors simultaneously. Dermoscopic examination of palmoplantar and intraumbilical lesions revealed a consistent, uniform appearance characterized by dot-like vessels and small lacunae across patients (Figure 19.) Given the monomorphic nature of these sites, they were excluded from the aforementioned dermoscopic structural evaluation.

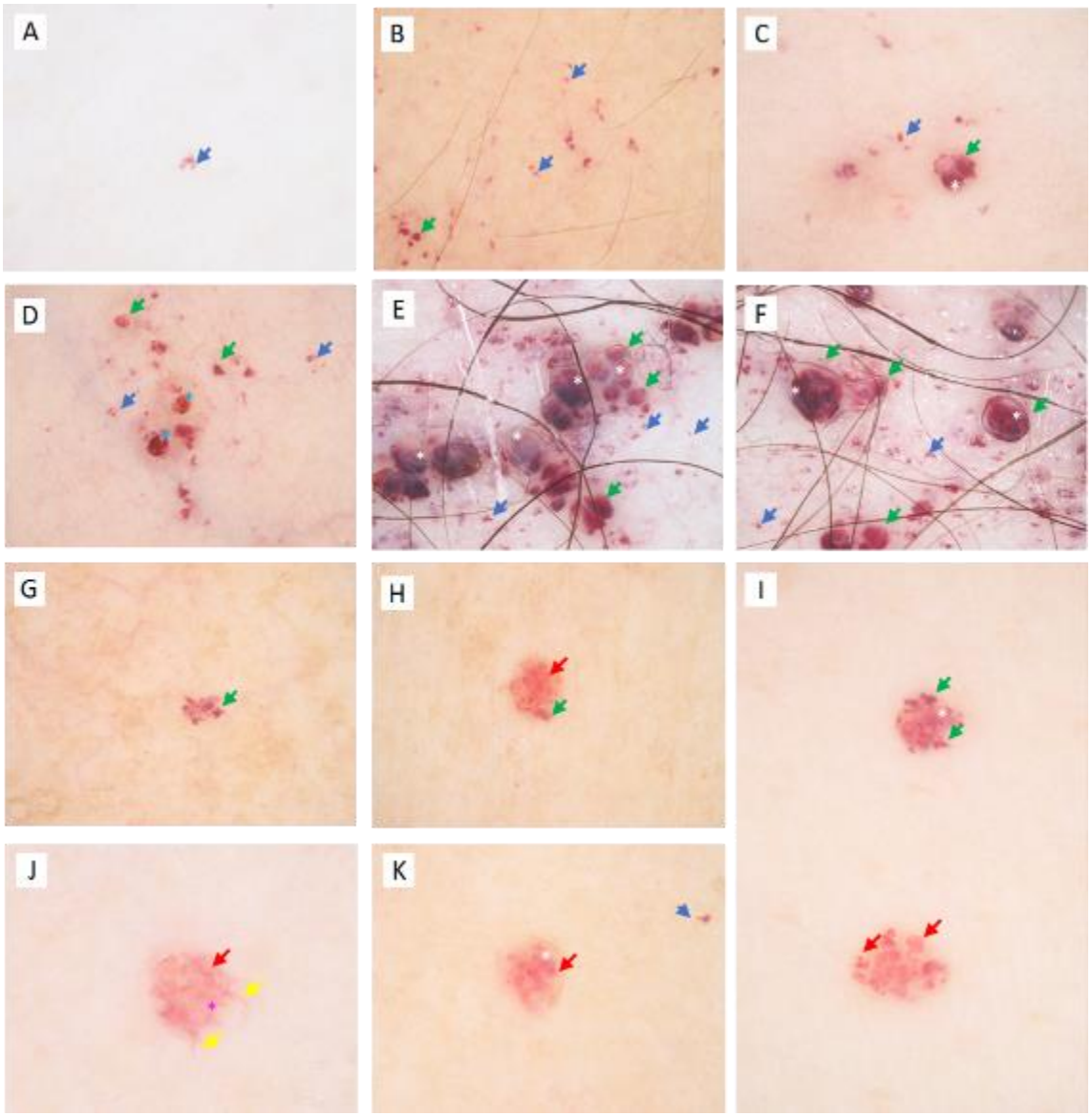

Figure 18. *Dermoscopic features of angiokeratomas in Fabry disease. Blue arrows: dot-like vessels, green arrows: red or purple lacunae, white asterisk: whitish veil, blue asterisk: crusting, red arrow: glomerular vessels, yellow arrow: linear-irregular vessels, pink asterisk: milky red areas. A: solitary, macular angiokeratoma on the upper arm of a young female patient B: diffuse macular angiokeratomas on the thigh of a young boy C: macular and papular angiokeratomas on the thigh of a young boy D: papular angiokeratomas with crusting on the thigh of a young boy E-F: papular, hyperkeratotic angiokeratomas among macular angiokeratomas on the trunk of male patients G: macular angiokeratoma on a female patient H-K: solitary, papular angiokeratomas on female patients localized on the upper trunk and arms*

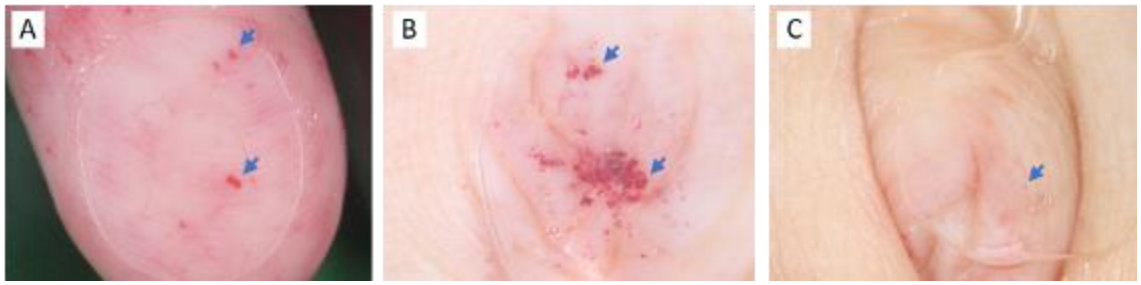

Figure 19. *Angiokeratomas on the fingertips (A) and in the umbilicus (B-C). Blue arrow: dot-like vessels.*

4.2.5. Dermoscopic features of other vascular structures

Apart from angiokeratomas, other vascular malformations such as hemangiomas and telangiectasias were frequently observed (Figure 20.). Distinguishing hemangiomas from angiokeratomas could be accomplished by identifying proliferative capillaries and white septae.

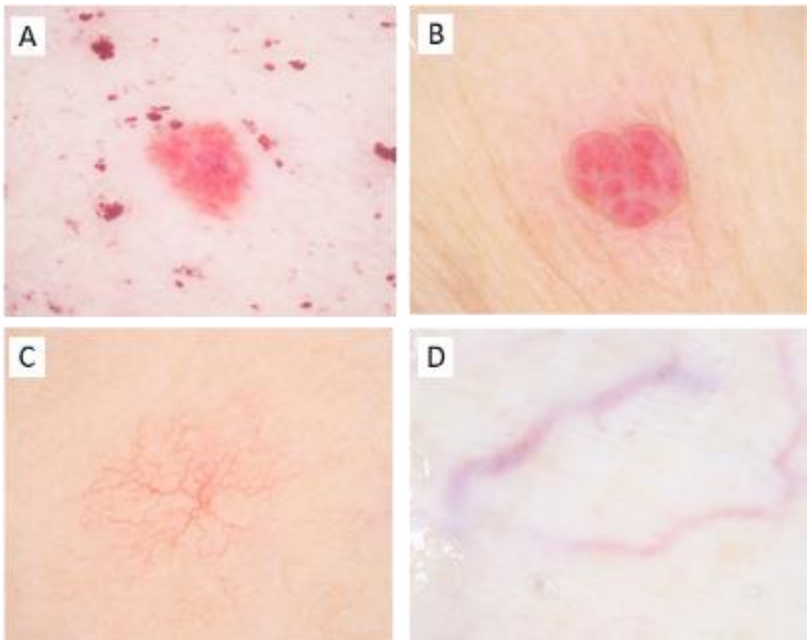

Figure 20. *Dermoscopy of other vascular lesions in Fabry disease. A: hemangioma among macular angiokeratomas on a male patient, B: hemangioma on a female patient, note the fibrous septae and bright red lacunae C: spider nevus on a young boy, D: dilated veins on the chest of a male patient.*

4.2.6. Nonlinear microscopy of angiokeratomas

Skin biopsies obtained from individuals diagnosed with FD were subjected to NLM evaluation to investigate the underlying pathological changes. Additionally, a biopsy sample of a hemangioma was utilized for the purpose of differential diagnosis. The skin tissue sections, previously preserved in formalin and embedded in paraffin, were deparaffinized and subjected to analysis using TPF and SHG techniques. Through this assessment, two-dimensional vertical cross-section mosaic images were acquired to emulate traditional histology. The SHG signal, displayed in magenta color, facilitated the visualization of collagen fibers within the dermal layer. Conversely, the TPF channel, depicted in green, highlighted the presence of keratinocytes in the epidermis, while the green lamellar structures corresponded to the stratum corneum in both samples. Notable morphological variations were observed, including hyperkeratosis and dilated blood vessels in the epidermis of angiokeratomas. Conversely, in the case of hemangioma, hyperkeratosis was absent, and the vasculature was not restricted to the epidermis and papillary dermis. Furthermore, the vessel morphology differed, characterized by smaller, proliferative capillaries (Figure 21.).

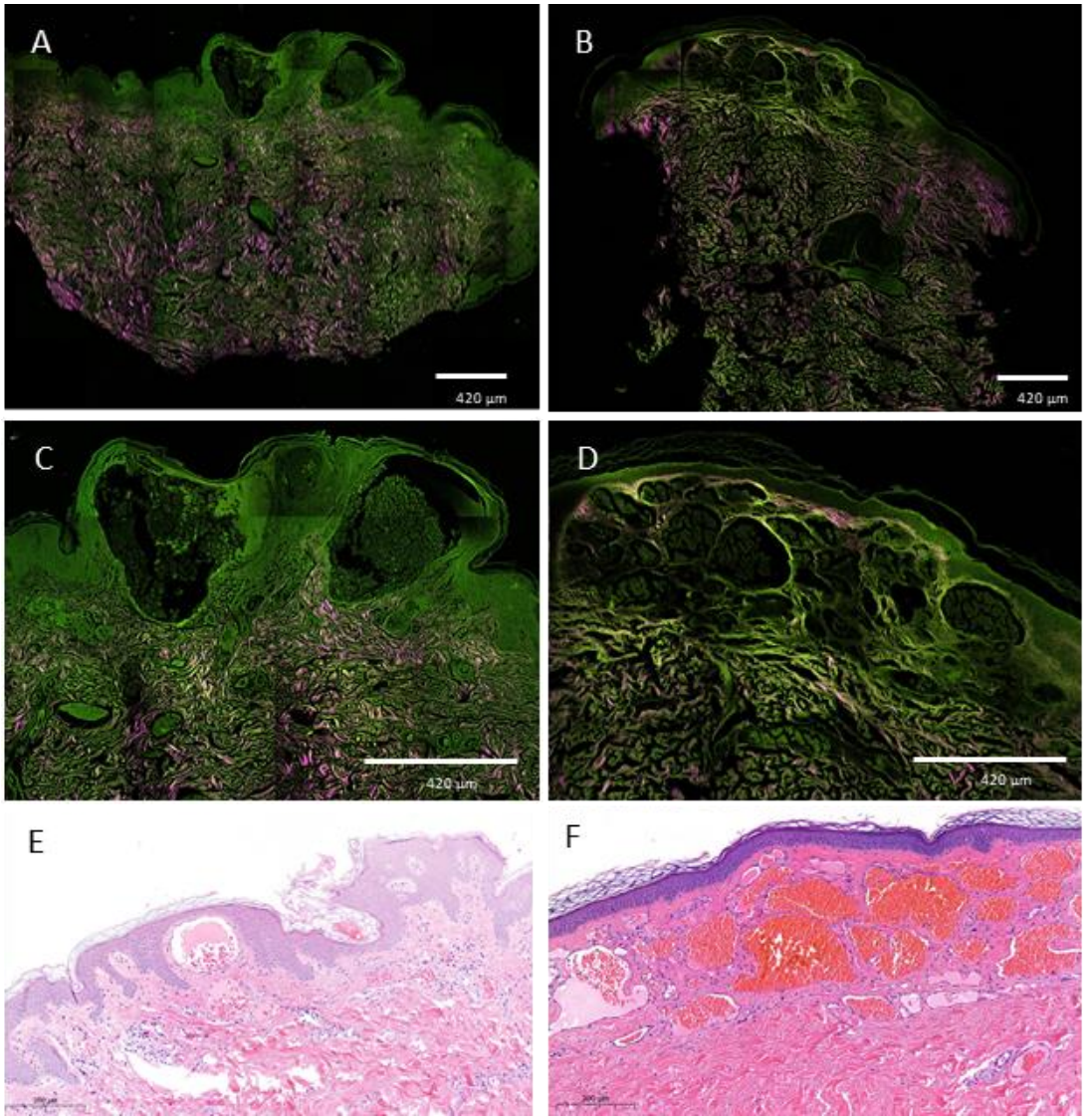

Figure 21. *Morphologic comparison of angiokeratoma and hemangioma with ex vivo nonlinear microscopy. Nonlinear microscopic images were captured for an angiokeratoma (A, C) obtained from our cohort of patients, as well as for a hemangioma serving as a reference for differential diagnosis (B, D). In the angiokeratoma sample (A, C), notable features included a hyperkeratotic surface and dilated capillaries primarily limited to the papillary dermis. Conversely, in the hemangioma sample, the capillaries extended further towards the subcutaneous tissues. The angiokeratoma displayed ectatic and dilated vessels (C), with a transition to normal vessel morphology upon descending deeper into the dermis. In contrast, the hemangioma sample was characterized by smaller-diameter vessels that were separated by thin fibrous septae (depicted as collagen fibers in pink) (D). Hematoxylin-eosin stained sections of the angiokeratoma (E) and*

hemangioma (F). The angiokeratoma features dilated vessels with acanthosis. The hemangioma presents with multiple vascular spaces and normal epithelium. Scale bar: 420 µm (A-D) 200 µm (E-F)

4.2.7. Multispectral imaging

Utilizing multispectral diffuse reflectance and autofluorescent imaging techniques, angiokeratomas are identifiable as regions of low intensity in comparison to the surrounding healthy skin, particularly evident in the green and autofluorescence channels. Notably, the subepidermal vasculature in the background is more discernible, especially in the autofluorescence channel, as well as in the green channel, compared to dermoscopic images (Figure 22.). When considering papular angiokeratomas, the affected areas demonstrate diminished signals of diffuse reflectance when using infrared illumination. On the other hand, macular angiokeratomas do not exhibit reduced diffuse reflectance under the same circumstances.

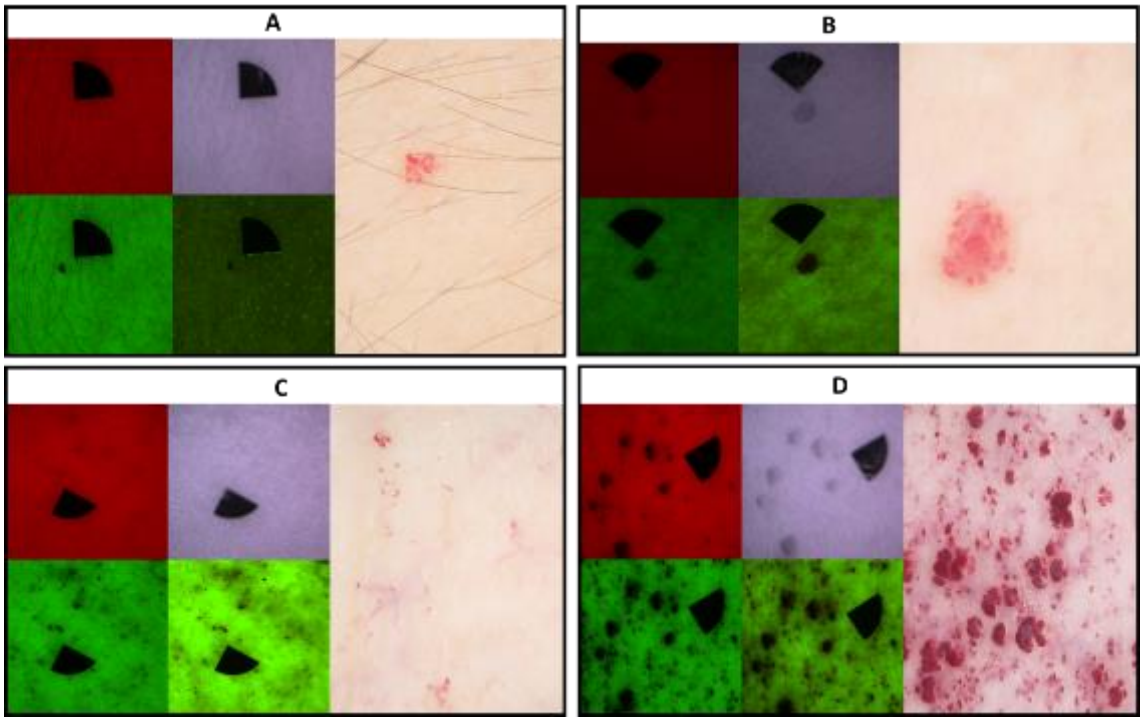

Figure 22. *Representative images of angiokeratomas with different morphologic features were captured using multispectral imaging, and a comparison was made with dermoscopic images of the selected lesions. A) solitary macular, B) solitary papular, C)*

clustered macular, and D) clustered papular and macular angiokeratomas. Each panel consisted of diffuse reflectance images at three different wavelengths: 663 nm (red light, upper left image), 526 nm (green light, lower left image), and 964 nm (infrared light, upper right image). Additionally, autofluorescence images were obtained using 405 nm light-emitting diode (LED) excitation (lower right pictures). Dermoscopic images were positioned on the right side of each panel to facilitate comparison.

5. DISCUSSION

Genodermatoses encompass a wide range of genetically inherited disorders that affect the skin. The diagnosis of genodermatoses often requires a multidisciplinary approach and the integration of clinical, laboratory, and genetic information. Genetic testing may include targeted mutation analysis, as done in FD and next-generation sequencing techniques, or chromosomal microarray analysis as utilized in the case of several ichthyoses. Next-generation sequencing has revolutionized genetic diagnostics by enabling simultaneous analysis of multiple genes associated with genodermatoses, providing a comprehensive approach to identify pathogenic mutations (36). Accurate diagnosis is essential for guiding appropriate management strategies, providing genetic counseling, and offering insights into the natural history of the condition. Novel advancements in genomic technologies and our understanding of genetic mutations associated with genodermatoses continue to enhance diagnostic accuracy, enabling earlier identification and intervention for affected individuals. It is important to note that the availability and affordability of genetic testing can vary depending on the specific condition and the healthcare setting. In some cases, genetic testing may not be readily accessible or may be reserved for specific situations where clinical suspicion is high.

In recent decades, significant advancements have been made in refining the diagnostic approaches for genodermatoses. Nonetheless, there remains a compelling interest in comprehending the optical changes of the skin associated with these diseases.

Optical imaging techniques have emerged as valuable tools in the diagnosis, monitoring, and management of various diseases in the field of dermatology. Non-invasive imaging methods could provide detailed information about the skin structure, function, and molecular composition, aiding in the understanding and characterization of various skin disorders.

Here, we used *in vivo* MSI and *ex vivo* NLM for the assessment of a keratinization disorder, a rare case of EI and FD, thus expanding the knowledge of the possible use of these tools in genodermatoses.

EI is a group of rare genetic diseases with diverse phenotypes caused by autosomal dominant mutations in suprabasal epidermal cytokeratin genes (*KRT1* or *KRT10*). EI

affects approximately 1 in 300,000 individuals, with 50% of cases resulting from inheritance and the remaining cases arising from *de novo* mutations (37). Our patient's parents lacked a history of keratinization disorder, and genetic analysis revealed no abnormalities in their allelic composition. Thus, it is likely that the patient acquired either a spontaneous mutation or a germline mutation from one of the parents. We identified a c.1436T>C mutation in the *KRT1* gene, resulting in an amino acid change from isoleucine to threonine in the helix termination motif (2B) of keratin 1. Mutations affecting such conserved regions are typically associated with severe forms of EI due to their importance in keratin assembly and filament formation. However, the c.1436T>C mutation has been reported to cause both severe and mild phenotypes of EI, including annular erythema ichthyosis (AEI, OMIM: 607602) (38, 39). Although AEI and major EI types share common initial symptoms at birth, such as blistering and erosions, they diverge in subsequent manifestations, with AEI displaying a milder phenotype (39). While our patient did not exhibit the typical features of AEI, which include recurrent episodes of annular erythematous lesions alternating with periods of near-clear skin, they did experience cutaneous symptoms characterized by intermittent relapses and remissions. The reported instances of the p.Ile479Thr mutation have been linked to severe palmoplantar keratoderma (PPK), regardless of the specific subtype of EI. Thus far, two families have been reported as exceptional cases of epidermolytic PPK, characterized by the presence of the identical *KRT1* mutation, in which cutaneous symptoms were relatively mild apart from PPK extending beyond the boundaries of the palms and soles (40). In contrast, typical epidermolytic PPK associated with *KRT9* mutations is characterized by hyperkeratosis limited to the palmoplantar surfaces, respecting their margins. Consistent with these reports, our patient's PPK worsened over time, and the same heterozygous 21-bp in-frame deletion in exon 9 of *KRT1*, Gly553-Tyr559del was observed in both the patient and his mother, similar to the two previously reported families with atypical PPK (40). This deletion is known to cause size polymorphism of keratin 1, with a frequency of 39% in the general population (35).The genotype-phenotype correlation in PPK within the context of EI is well-established, primarily associated with *KRT1* mutations rather than *KRT10* mutations (41). However, our case suggests that the correlation between genotype and other skin manifestations, such as hyperkeratosis, blistering, erythema, and disease severity, is not consequent. The

observed weak association is hypothesized to be influenced by yet undisclosed genetic and epigenetic factors (39). Although genetic testing is the primary method for diagnosing ichthyoses, conventional histology is commonly utilized as a supplementary approach in cases where genetic analysis is inconclusive or inaccessible. Our study aimed to explore alternative optical imaging modalities for the diagnosis of keratinization disorders, in addition to conventional histology. Keratins, along with lipids, collagen, and elastin, are significant fluorophores in the skin, making them suitable targets for imaging techniques The optical properties of skin, including light absorption and emission, are significantly influenced by the composition, distribution, and abundance of fluorophores and chromophores. Consequently, biological processes that alter these fluorophores and chromophores can lead to changes in the optical properties of the tissue (42). The investigation of changes in tissue autofluorescence has garnered significant attention in the context of skin cancer research and diagnostics (25, 28, 32, 43). Moreover, its application is gradually expanding to encompass the research of rare diseases such as pseudoxanthoma elasticum (26). Autofluorescence imaging under narrow-band LED illumination was used to compare skin lesions in our patient with a healthy control. Hyperkeratosis exhibited a strong autofluorescence signal under 405 nm LED excitation, attributed to the abundance of keratin (44). However, it is worth noting that the entirety of the signal may not originate solely from keratin, as other fluorophores such as lipids may also be implicated (45). While the precise mechanism behind the heightened autofluorescence is uncertain, the impact of hyperkeratosis on intrinsic autofluorescence alterations was significant in our case. Autofluorescence patterns in skin samples with varying keratin content, including hand callus, palmar skin, and thin forearm skin were investigated under different excitation wavelengths (46). Emission and excitation scans revealed notable differences between forearm skin and callus, primarily attributed to increased keratin content, while normal thickness palmar skin and callus displayed similar autofluorescence patterns (46). Alterations in autofluorescence have been observed in the context of inflammatory skin diseases, including psoriasis and atopic dermatitis, when examined using 408 nm LED excitation. These studies have demonstrated the utility of autofluorescence as a valuable tool for enhancing diagnostic accuracy. Specifically, the heightened autofluorescence intensity observed in psoriasis has been attributed to abnormal keratinization, along with other contributing factors such as elevated levels of

involucrin and increased collagen production, as suggested by the authors (47). However, it is noteworthy to mention that autofluorescence signals generated by LED excitation originate from different tissue layers, potentially causing interference (48). The presence of a hyperkeratotic epithelial layer can potentially diminish the autofluorescence signal from the underlying tissue by impeding the penetration of the excitation light (44). NLM can overcome this limitation by providing optical sectioning, allowing the separation of autofluorescence signals from different tissue layers. Different NLM techniques, such as TPF and SHG, enable selective visualization of various tissue components. However, the substantial thickness of hyperkeratosis in our plantar keratoderma sample greatly hindered the depth of penetration. While the papillary dermis was discernible in the vertical images of the skin section, it was inaccessible through horizontal optical sectioning of the fresh skin biopsy sample due to the scattering effect caused by keratin. In the healthy control, the normal structure of the epidermis enabled clear visualization of the papillary dermis, thus this approach holds potential value in diagnosing cutaneous disorders that do not involve a hyperkeratotic epidermis. While obtaining a biopsy is necessary for vertical imaging using NLM, it offers a more intricate depiction of the corneal layer in comparison to traditional histology. Consequently, it holds potential value in diseases that impact the stratum corneum.

In the context of FD, MSI was also employed, with the inclusion of more excitation wavelengths. Autofluorescent and green light excitation, where the absorption of hemoglobin played a significant role, allowed enhanced distinction of the background vasculature compared to dermoscopy. However, it should be noted that the imaging device utilized in this study had lower resolution and magnification capabilities, resulting in less detailed visualization of vascular structures. In addition to the wavelengths used in the EI case, we also incorporated infrared and red excitation. Specifically, under infrared illumination, papular angiokeratomas exhibited regions of low diffuse reflectance signals, potentially indicating deeper involvement of the lesions. Similar observations were made in cases of melanomas with varying degrees of invasion depth (49). In the case of NLM investigations in the context of FD, we only utilized paraffinized and deparaffinized angiokeratoma samples for vertical imaging. In contrast to the EI case, a 525/50 nm (green) bandpass filter was used for the detection of the TPF signal instead of a 590/45 nm (orange) filter based on preliminary measurements on native blood, where

blood cells showed strong TPF signal. Using morphological features akin to conventional hematoxylin-eosin staining, we were able to distinguish between angiokeratomas and hemangiomas. Notably, in our experimental setup, vascular spaces appeared as black lumens due to the specific sample preparation procedure. To simulate an *in vivo* imaging approach without potential modifications from paraffination and deparaffination procedures, the use of fresh frozen samples could be considered as seen in our EI case.

In addition to the evaluation of these optical imaging modalities, we also aimed to examine the clinical heterogeneity and diagnostic challenges of FD from a dermatologist perspective and also to evaluate the dermoscopic findings of angiokeratomas in our FD patient cohort.

FD is the most common lysosomal storage disease with a clinically heterogeneous presentation regarding both cutaneous and extracutaneous manifestations. The diverse clinical presentation of the disease can contribute to delays in diagnosis, thereby hindering the prompt initiation of disease-specific treatment. In the absence of appropriate interventions, the disease can progress to a state of advanced organ dysfunction, ultimately resulting in end-organ damage and premature mortality. Skin manifestations occur frequently and typically serve as an early indication of the disease, underscoring the pivotal role of accurate assessment of cutaneous signs in facilitating early suspicion of FD. ACDU is considered the primary cutaneous manifestation of FD, although less common cutaneous signs such as abnormalities in sweating, other vascular lesions, and facial dysmorphia may also be observed. In our cohort of patients, the prevalence of angiokeratomas was higher, with 92% of patients exhibiting this condition, compared to the literature where angiokeratomas were observed in 69% of patients (15). In our patient group, we observed a higher likelihood of angiokeratomas occurring in the typical bathing suit distribution in males, whereas females predominantly exhibited angiokeratomas on their trunk and extremities, which aligns with existing literature on the subject (50). Based on our findings, a mere 38% of our patient group, predominantly males, exhibited multiple clustered angiokeratomas in the bathing suit distribution. The remaining approximately two-thirds of the patients either displayed minimal or no angiokeratomas, or showcased atypical angiokeratomas in terms of their distribution and appearance. These findings indicate that slightly over one-third of our cohort exhibited the clinically evident phenotype of ACDU, while the majority of cases presented with less conspicuous

features that could pose a challenge for diagnosis. This observation emphasizes the extensive variability in the presentation of angiokeratomas in FD beyond the classic manifestation of ACDU. Furthermore, irrespective of their distribution, incipient, macular angiokeratomas are less perceptible and may be inadvertently disregarded without a comprehensive dermatological evaluation or by less proficient practitioners, leading to a delay in diagnosis. While we observed great clinical variability regarding the distribution, number and morphology of angiokeratomas, we could observe intrafamilial resemblances. Specifically, a mother and her son, as well as a family of middle-aged brothers, displayed only a limited number of angiokeratomas (<5) outside of the bathing suit distribution. In another family, two middle-aged brothers showed incipient angiokeratomas in the bathing suit distribution.

Although most individuals in our patient cohort exhibited an atypical form of ACDU, it is noteworthy that this group also displayed additional cutaneous manifestations of FD, such as hypohidrosis. Consequently, the coexistence of these less apparent/distinctive cutaneous signs, in conjunction with extracutaneous manifestations, holds the potential to facilitate the recognition of the disease, even in the absence of the characteristic ACDU presentation.

Hypohidrosis was seen in 42% of our patients affecting 21.4% of female patients and 66.7% of male patients, aligning closely with the prevalence rates reported in the existing literature (17). Hyperhidrosis was present in 30.8% of our patients affecting 35.7% of women and 16.7% of men. Consistent with previous studies, a higher prevalence of hyperhidrosis was noted among women in the literature. However, in our specific patient group, the occurrence of hyperhidrosis was even more frequent (17). Telangiectases were observed in 57.7% of our patient group, affecting 50% of males and 64.3% of female patients, which was higher than in the literature (17).

In our study, we identified synophrys in 16% of the cases and propose it as a novel cutaneous manifestation of FD. Although synophrys can be considered a normal variant in certain ethnicities (51), it may also indicate the presence of other lysosomal disorders (52). Furthermore, varicose veins were identified in nearly half of our patient cohort, including two younger individuals of 12-14 years of age as well. The occurrence of varicose veins showed an equal gender distribution in our group in contrast to the general

population where a female predominance can be seen (53). To our knowledge, only two case reports have previously documented the presence of varicose veins in FD. In one instance, a patient exhibited bilateral leg ulcers at an early age, and upon venography, venous reflux and varicose veins were observed. Subsequent investigation of the family history led to the diagnosis of FD (54). In another case report, the presence of lower extremity varicose veins was only briefly mentioned (55). Although the impact of Gb3 accumulation on venous tissue remains insufficiently explored, our hypothesis suggests that venous insufficiency in the lower extremities could be a prevalent yet overlooked manifestation of FD.

We conducted an analysis of 135 dermoscopic images of angiokeratomas in 24 patients, which, to the best of our knowledge, represents the most extensive collection of such images in the literature. The angiokeratomas in our cohort were predominantly characterized by the presence of dark red lacunae, with a frequent occurrence of dot-like vessels. Notably, we observed that the whitish veil, previously reported to be present in 77% of cases according to the literature (56), was only found in 25% of our cases. The reason for this low frequency could be due to the large number of incipient, macular angiokeratomas in our group. However, it is important to acknowledge that dermoscopy exhibited considerable variability in the assessment of these lesions, particularly in the case of atypical and solitary angiokeratomas, where glomerular and irregular vascular structures were more commonly observed. Overall, dermoscopy proved to be a valuable tool for the examination of early-stage macular angiokeratomas and for the evaluation of lesions in the navel.

The emergence of disease-specific therapies created a need for assessing their effectiveness, and skin manifestations could potentially be a viable option for evaluating treatment outcomes due to their easy accessibility. However, the literature regarding the impact of ERT on angiokeratomas is conflicting. Electron microscopy revealed the complete elimination of Gb3 from the superficial capillary endothelium in the skin after five months of ERT (57). However, the impact of enzyme replacement therapy on the vasculopathy observed in FD seems to be minimal. Although prolonged ERT has the potential to halt the advancement of angiokeratomas and may promote partial regression, the complete resolution of angiokeratomas should not be anticipated (18). Nevertheless, there have been instances where angiokeratomas exhibited remission following long-term

therapy (58), so the monitoring of angiokeratomas for the evaluation of treatment might not be feasible.

Overall, our studies provide insights into different genetic skin diseases, their clinical manifestations, challenges in genotype-phenotype correlations, and potential diagnostic approaches. They underscore the importance of multidisciplinary care involving genetic testing, counseling, and specialized imaging techniques in improving the diagnosis and management of these disorders.

We implemented *ex vivo* NLM and *in vivo* MSI to visualize keratin in a rare case of KPI. NLM offers high-resolution imaging at the cellular level, with the ability to optically section the sample. However, the presence of hyperkeratosis can impede NLM imaging when using fresh biopsy samples. Additionally, the high cost of NLM limits its accessibility to a small number of facilities. As an alternative, autofluorescence imaging under narrow-band LED excitation presents a cost-effective and user-friendly *in vivo* method for diagnosing keratinization disorders.

Angiokeratomas serve as crucial indicators of FD and play a significant role in screening and establishing its diagnosis. The prompt identification of the disease is vital to halt its progression and avert potentially life-threatening complications. The presence of diffuse angiokeratomas should raise suspicion among physicians, prompting further investigation for FD or other storage disorders. Nevertheless, our observations in the patient group, particularly among females, revealed instances where angiokeratomas exhibited an atypical distribution, affecting various skin sites and manifesting as solitary lesions instead of clustered formations, thereby posing challenges in diagnosis. We wish to underscore the importance of employing dermoscopy as a valuable diagnostic tool, as it enables the detection of incipient angiokeratomas and intraumbilical angiokeratomas that might otherwise be overlooked. Furthermore, emerging optical modalities such as MSI and NLM hold promise in facilitating the diagnosis of atypical cases.

6. CONCLUSIONS

- We utilized MSI in a case of EI caused by *KRT1* gene mutation. When subjected to 405 nm LED excitation, hyperkeratosis showed a higher autofluorescence response compared to healthy skin.
- We used *ex vivo* NLM modalities with a particular focus on the visualization of alterations brought on by epidermolytic hyperkeratosis. In the case of horizontal imaging with NLM on fresh frozen EI biopsy sample, the presence of thick hyperkeratosis and the strong autofluorescence of keratin posed challenges in visualizing the papillary dermis. The assessment of vertical sections of the EI with NLM provides a detailed label-free imaging of the epidermal layers.
- Upon the MSI assessment of angiokeratomas in FD, angiokeratomas can be recognized as areas of reduced intensity compared to the surrounding healthy skin, which is particularly noticeable under 526nm and 405 nm LED illumination. It is worth noting that the subepidermal blood vessels in the background are more distinguishable, particularly in these channels, in contrast to dermoscopic images. Additionally, upon 964 nm infrared illumination of papular angiokeratomas, the lesions display diminished diffuse reflectance signals. In contrast, macular incipient angiokeratomas do not exhibit reduced diffuse reflectance under the same circumstances, which might be due to the thickness of the lesion.
- We assessed an angiokeratoma from a FD patient and a hemangioma from a healthy control with *ex vivo* NLM. We observed significant differences in morphology, the angiokeratoma exhibited hyperkeratosis and ectatic, enlarged blood vessels within the epidermis. In contrast, the hemangioma lacked hyperkeratosis and the vasculature characterized by smaller, proliferative capillaries was not limited to the epidermis and papillary dermis.
- Angiokeratomas were present in 92% of our FD patient cohort, which was a considerably higher ratio compared to the literature. Only 38% of the patients, mainly males, presented the typical form of ACDU in the bathing suit distribution. While the majority of individuals in our group of patients presented angiokeratomas in an atypical distribution or appearance.

- Dermoscopy can have a notable benefit in the assessment of incipient angiokeratomas. While dermoscopic images of angiokeratomas also showed great variability. Angiokeratomas in our patient group primarily showed the presence of dark red lacunae, often accompanied by dot-like vascular structures. The whitish veil corresponding to hyperkeratosis was only observed in 25% of our cases, which was considerably less frequent, than reported in the literature.

7. SUMMARY

Although notable advancements have been made in improving the diagnostic methods for genodermatoses, there remains a strong interest in understanding the optical changes in the skin in these conditions. Diseases affecting the fluorophores of the skin can alter its optical properties. Optical imaging modalities are invaluable tools in dermatology for diagnosis, monitoring, and treatment. We assessed a rare case of EI and a cohort of FD patients using MSI and NLM. In the case of EI, the autofluorescence intensity in the thickened skin on the palms was significantly higher than in healthy skin. Using NLM for vertical imaging on fresh frozen EI biopsy samples posed challenges in visualizing the papillary dermis due to the hyperkeratotic epidermis. Nevertheless, NLM provided comprehensive visualization of the epidermal layers. During the assessment of angiokeratomas in FD using MSI, subepidermal blood vessels in the background were more distinguishable, particularly in the 405 nm autofluorescence and 526 nm green channels, compared to dermoscopic images. Papular angiokeratomas exhibited decreased diffuse reflectance signals under 964 nm infrared illumination, while macular angiokeratomas did not display such reduction, potentially due to lesion thickness. Using NLM, we observed notable morphological differences between the angiokeratoma and hemangioma samples. The angiokeratoma showed hyperkeratosis and enlarged blood vessels within the epidermis, whereas the hemangioma lacked hyperkeratosis, and the vasculature extended beyond the epidermis and papillary dermis. In our FD patient cohort, we observed more angiokeratomas compared to the literature data. However, we noticed significant clinical variability in the appearance and distribution of angiokeratomas. Males often presented clusters of angiokeratomas in the bathing suit distribution, while females tended to have solitary angiokeratomas on the trunk and extremities. We evaluated 135 dermoscopic images of angiokeratomas. Dark red lacunae and dot-like vascular structures were the most frequently observed structures, while the whitish veil was present in a considerably lower fraction of cases compared to the literature. Only 38% of patients, mostly males, showed the typical form of ACDU. The majority of patients presented with unconventional forms of ACDU or minimal/no angiokeratomas but displayed other skin signs of FD. These additional skin manifestations can aid the diagnosis even in the absence of characteristic ACDU.

8. REFERENCES

1. Richter T, Nestler-Parr S, Babela R, Khan ZM, Tesoro T, Molsen E, Hughes DA. Rare Disease Terminology and Definitions—A Systematic Global Review: Report of the ISPOR Rare Disease Special Interest Group. Value in Health. 2015;18(6):906-914.
2. Aşkın Ö, Engin B, Gencebay G, Tüzün Y. A multistep approach to the diagnosis of rare genodermatoses. Clin Dermatol. 2020;38(4):399-407.
3. Fischer J, Bourrat E. Genetics of Inherited Ichthyoses and Related Diseases. Acta Derm Venereol. 2020;100(7):adv00096.
4. Elias PM, Gruber R, Crumrine D, Menon G, Williams ML, Wakefield JS, Holleran WM, Uchida Y. Formation and functions of the corneocyte lipid envelope (CLE). Biochim Biophys Acta. 2014;1841(3):314-318.
5. Vahlquist A, Fischer J, Törmä H. Inherited Nonsyndromic Ichthyoses: An Update on Pathophysiology, Diagnosis and Treatment. Am J Clin Dermatol. 2018;19(1):51-66.
6. Anker P, Medvecz M. Ichthyosisok patogenezise: a terminális differenciáció zavarai. Bőrgy Vener Szeml. 2020;96(1):3-10.
7. Pinkova B, Buckova H, Borska R, Fajkusova L. Types of congenital nonsyndromic ichthyoses. Biomed Pap Med Fac Univ Palacky Olomouc Czech Repub. 2020;164(4):357-365.
8. Oji V, Preil ML, Kleinow B, Wehr G, Fischer J, Hennies HC, Hausser I, Breitkreutz D, Aufenvenne K, Stieler K, Tantcheva-Poór I, Weidinger S, Emmert S, Hamm H, Perusquia-Ortiz AM, Zaraeva I, Diem A, Giehl K, Fölster-Holst R, Kiekbusch K, Höger P, Ott H, Traupe H. S1 guidelines for the diagnosis and treatment of ichthyoses - update. J Dtsch Dermatol Ges. 2017;15(10):1053-1065.
9. Medvecz M, Anker P, Pálla S, Plázár D, Farkas K, Kiss N, Becker K. Clinical and genetic aspects of inherited ichthyoses. Bőrgy Vener Szeml. 2022;98(2):44-54.
10. Chulpanova DS, Shaimardanova AA, Ponomarev AS, Elsheikh S, Rizvanov AA, Solovyeva VV. Current Strategies for the Gene Therapy of Autosomal Recessive Congenital Ichthyosis and Other Types of Inherited Ichthyosis. Int J Mol Sci. 2022;23(5).
11. Spada M, Pagliardini S, Yasuda M, Tukel T, Thiagarajan G, Sakuraba H, Ponzone A, Desnick RJ. High incidence of later-onset fabry disease revealed by newborn screening. Am J Hum Genet. 2006;79(1):31-40.

12. Miller JJ, Kanack AJ, Dahms NM. Progress in the understanding and treatment of Fabry disease. Biochim Biophys Acta Gen Subj. 2020;1864(1):129437.
13. Wittmann J, Karg E, Turi S, Legnini E, Wittmann G, Giese AK, Lukas J, Gölnitz U, Klingenhäger M, Bodamer O, Mühl A, Rolfs A. Newborn screening for lysosomal storage disorders in hungary. JIMD Rep. 2012;6:117-125.
14. van der Veen SJ, Hollak CEM, van Kuilenburg ABP, Langeveld M. Developments in the treatment of Fabry disease. J Inherit Metab Dis. 2020;43(5):908-921.
15. Dutra-Clarke M, Tapia D, Curtin E, Rünger D, Lee GK, Lakatos A, Alandy-Dy Z, Freedkin L, Hall K, Ercelen N, Alandy-Dy J, Knight M, Pahl M, Lombardo D, Kimonis V. Variable clinical features of patients with Fabry disease and outcome of enzyme replacement therapy. Mol Genet Metab Rep. 2020;26:100700.
16. Lenders M, Brand E. Fabry Disease: The Current Treatment Landscape. Drugs. 2021;81(6):635-645.
17. Orteu CH, Jansen T, Lidove O, Jaussaud R, Hughes DA, Pintos-Morell G, Ramaswami U, Parini R, Sunder-Plassman G, Beck M, Mehta AB. Fabry disease and the skin: data from FOS, the Fabry outcome survey. Br J Dermatol. 2007;157(2):331-337.
18. Merzel Šabović EK, Žerjav Tanšek M, Grošelj U, Dragoš V. Angiokeratomas and treatment with enzyme replacement therapy in a patient with Fabry disease. Acta Dermatovenerol Alp Pannonica Adriat. 2020;29(2):89-91.
19. Piccolo V, Russo T, Moscarella E, Brancaccio G, Alfano R, Argenziano G. Dermatoscopy of Vascular Lesions. Dermatol Clin. 2018;36(4):389-395.
20. Vadher P, Agarwal P, Mistry A, Gajjar K, Bansal N, Neazee S. Angiokeratoma Corporis Diffusum: An Uncommon Case with Suspected Anderson Fabry Disease. Indian Dermatol Online J. 2020;11(2):212-215.
21. Lidove O, Ramaswami U, Jassaud R, Barbey F, Maisonobe T, Caillaud C, Beck M, Sunder-Plassmann G, Linhart A, Mehta A. Hyperhidrosis: a new and often early symptom in Fabry disease. International experience and data from the Fabry Outcome Survey. Int J Clin Pract. 2006;60(9):1053-1059.
22. Ashique KT, Kaliyadan F, Aurangabadkar SJ. Clinical photography in dermatology using smartphones: An overview. Indian Dermatol Online J. 2015;6(3):158-163.

23. Chauhan P, Meena D, Errichetti E. Dermoscopy of Bacterial, Viral, and Fungal Skin Infections: A Systematic Review of the Literature. Dermatol Ther (Heidelb). 2023;13(1):51-76.

24. Sonthalia S, Agrawal M, Bhatia J, Zeeshan M, Elsamanoudy S, Tiwary P, Bhat YJ, Jha A, Bosseila M. Entodermoscopy Update: A Contemporary Review on Dermoscopy of Cutaneous Infections and Infestations. Indian Dermatol Online J. 2021;12(2):220-236.

25. Bozsányi S, Farkas K, Bánvölgyi A, Lőrincz K, Fésűs L, Anker P, Zakariás S, Jobbágy A, Lihacova I, Lihachev A, Lange M, Bliznuks D, Medvecz M, Kiss N, Wikonkál NM. Quantitative Multispectral Imaging Differentiates Melanoma from Seborrheic Keratosis. Diagnostics (Basel). 2021;11(8):1315.

26. Farkas K, Bozsányi S, Plázár D, Bánvölgyi A, Fésűs L, Anker P, Zakariás S, Lihacova I, Lihachev A, Lange M, Arányi T, Wikonkál NM, Medvecz M, Kiss N. Autofluorescence Imaging of the Skin Is an Objective Non-Invasive Technique for Diagnosing Pseudoxanthoma Elasticum. Diagnostics (Basel). 2021;11(2):260.

27. Cicchi R, Kapsokalyvas D, Pavone FS. Clinical nonlinear laser imaging of human skin: a review. Biomed Res Int. 2014;2014:903589.

28. Kiss N, Haluszka D, Lőrincz K, Gyöngyösi N, Bozsányi S, Bánvölgyi A, Szipőcs R, Wikonkál N. Quantitative Analysis on Ex Vivo Nonlinear Microscopy Images of Basal Cell Carcinoma Samples in Comparison to Healthy Skin. Pathol Oncol Res. 2019;25(3):1015-1021.

29. Kiss N, Fésűs L, Bozsányi S, Szeri F, Van Gils M, Szabó V, Nagy AI, Hidvégi B, Szipőcs R, Martin L, Vanakker O, Arányi T, Merkely B, Wikonkál NM, Medvecz M. Nonlinear optical microscopy is a novel tool for the analysis of cutaneous alterations in pseudoxanthoma elasticum. Lasers Med Sci. 2020;35(8):1821-1830.

30. Kiss N, Haluszka D, Lőrincz K, Kuroli E, Hársing J, Mayer B, Kárpáti S, Fekete G, Szipőcs R, Wikonkál N, Medvecz M. Ex vivo nonlinear microscopy imaging of Ehlers-Danlos syndrome-affected skin. Arch Dermatol Res. 2018;310(5):463-473.

31. König K, Breunig HG, Batista A, Schindele A, Zieger M, Kaatz M. Translation of two-photon microscopy to the clinic: multimodal multiphoton CARS tomography of in vivo human skin. J Biomed Opt. 2020;25(1):1-12.

32. Lihachev A, Derjabo A, Ferulova I, Lange M, Lihacova I, Spigulis J. Autofluorescence imaging of basal cell carcinoma by smartphone RGB camera. J Biomed Opt. 2015;20:120502.

33. Lihachev A, Lihacova I, Plorina EV, Lange M, Derjabo A, Spigulis J. Differentiation of seborrheic keratosis from basal cell carcinoma, nevi and melanoma by RGB autofluorescence imaging. Biomed Opt Express. 2018;9(4):1852-1858.

34. Errichetti E, Zalaudek I, Kittler H, Apalla Z, Argenziano G, Bakos R, Blum A, Braun RP, Ioannides D, Lacarrubba F, Lazaridou E, Longo C, Micali G, Moscarella E, Paoli J, Papageorgiou C, Russo T, Scope A, Stinco G, Thomas L, Toncic RJ, Tschandl P, Cabo H, Hallpern A, Hofmann-Wellenhof R, Malvehy J, Marghoob A, Menzies S, Pellacani G, Puig S, Rabinovitz H, Rudnicka L, Vakirlis E, Soyer P, Stolz W, Tanaka M, Lallas A. Standardization of dermoscopic terminology and basic dermoscopic parameters to evaluate in general dermatology (non-neoplastic dermatoses): an expert consensus on behalf of the International Dermoscopy Society. Br J Dermatol. 2020;182(2):454-467.

35. Korge BP, Compton JG, Steinert PM, Mischke D. The two size alleles of human keratin 1 are due to a deletion in the glycine-rich carboxyl-terminal V2 subdomain. J Invest Dermatol. 1992;99(6):697-702.

36. Chiu FP, Doolan BJ, McGrath JA, Onoufriadis A. A decade of next-generation sequencing in genodermatoses: the impact on gene discovery and clinical diagnostics. Br J Dermatol. 2021;184(4):606-616.

37. Lacz NL, Schwartz RA, Kihiczak G. Epidermolytic hyperkeratosis: a keratin 1 or 10 mutational event. Int J Dermatol. 2005;44(1):1-6.

38. Sybert VP, Francis JS, Corden LD, Smith LT, Weaver M, Stephens K, McLean WH. Cyclic ichthyosis with epidermolytic hyperkeratosis: A phenotype conferred by mutations in the 2B domain of keratin K1. Am J Hum Genet. 1999;64(3):732-738.

39. Reolid A, Carrasco L, Noguera-Morel L, Torrelo A, Colmenero I, Ortiz-Cabrera NV, Hernández-Martin Á. Annular epidermolytic ichthyosis: An exceptional mild subtype of epidermolytic ichthyosis without genotype and phenotype correlation. JAAD Case Rep. 2019;6(1):46-50.

40. Terron-Kwiatkowski A, Terrinoni A, Didona B, Melino G, Atherton DJ, Irvine AD, McLean WH. Atypical epidermolytic palmoplantar keratoderma presentation associated with a mutation in the keratin 1 gene. Br J Dermatol. 2004;150(6):1096-1103.

41. Hotz A, Oji V, Bourrat E, Jonca N, Mazereeuw-Hautier J, Betz RC, Blume-Peytavi U, Stieler K, Morice-Picard F, Schonbuchner I, Markus S, Schlipf N, Fischer J. Expanding the Clinical and Genetic Spectrum of KRT1, KRT2 and KRT10 Mutations in Keratinopathic Ichthyosis. Acta Derm Venereol. 2016;96(4):473-478.

42. Bliznakova I, Borisova E, Avramov L. Laser- and Light-Induced Autofluorescence Spectroscopy of Human Skin in Dependence on Excitation Wavelengths. Acta Physica Polonica A. 2007;112(5):1131-1136.

43. Lihacova I, Bolochko K, Plorina EV, Lange M, Lihachev A, Bliznuks D, Derjabo A. A method for skin malformation classification by combining multispectral and skin autofluorescence imaging: SPIE; 2018.

44. Wu Y, Qu JY. Autofluorescence spectroscopy of epithelial tissues. J Biomed Opt. 2006;11(5):054023.

45. Zheng W, Wu Y, Li D, Qu JY. Autofluorescence of epithelial tissue: single-photon versus two-photon excitation. J Biomed Opt. 2008;13(5):054010.

46. Rick AD, Howard ES, Peter GS, Robert RA, Stimson PSMD, editors. Influence of keratin on native cellular fluorescence of human skin. Photonics West '96; 1996; San Jose, California, United States: SPIE.

47. Yim JH, Jeong KH, Shin MK. Comparative study of skin autofluorescence expression in atopic dermatitis and psoriasis: A prospective in vivo study. Skin Res Technol. 2017;23(2):169-175.

48. Wu Y, Xi P, Qu JY, Cheung T-H, Yu M-Y. Depth-resolved fluorescence spectroscopy reveals layered structure of tissue. Opt Express. 2004;12(14):3218-3223.

49. Bozsányi S, Varga NN, Farkas K, Bánvölgyi A, Lőrincz K, Lihacova I, Lihachev A, Plorina EV, Bartha Á, Jobbágy A, Kuroli E, Paragh G, Holló P, Medvecz M, Kiss N, Wikonkál NM. Multispectral Imaging Algorithm Predicts Breslow Thickness of Melanoma. J Clin Med. 2021;11(1):189.

50. Chan B, Adam DN. A Review of Fabry Disease. Skin Ther Lett. 2018;23(2):4-6.

51. Kumar P. Synophrys: Epidemiological Study. Int J Trichology. 2017;9(3):105-107.

52. Galimberti C, Madeo A, Di Rocco M, Fiumara A. Mucopolysaccharidoses: early diagnostic signs in infants and children. Ital J Pediatr. 2018;44(Suppl 2):133.

53. Beebe-Dimmer JL, Pfeifer JR, Engle JS, Schottenfeld D. The Epidemiology of Chronic Venous Insufficiency and Varicose Veins. Ann Epidem. 2005;15(3):175-184.
54. Okada J, Hossain MA, Wu C, Miyajima T, Yanagisawa H, Akiyama K, Eto Y. Ten-year-long enzyme replacement therapy shows a poor effect in alleviating giant leg ulcers in a male with Fabry disease. Mol Genet Metab Rep. 2018;14:68-72.
55. Śnit M, Przyłudzka M, Grzeszczak W. Fabry disease - a genetically conditioned extremely rare disease with a very unusual course. Intractable Rare Dis Res. 2022;11(1):34-36.
56. Gao J, Fei W, Shen C, Shen X, Sun M, Xu N, Li Q, Huang C, Zhang T, Ko R, Cui Y, Yang C. Dermoscopic Features Summarization and Comparison of Four Types of Cutaneous Vascular Anomalies. Front Med (Lausanne). 2021;8:692060.
57. Thurberg BL, Randolph Byers H, Granter SR, Phelps RG, Gordon RE, O'Callaghan M. Monitoring the 3-Year Efficacy of Enzyme Replacement Therapy in Fabry Disease by Repeated Skin Biopsies. J Invest Dermatol. 2004;122(4):900-908.
58. Furujo M, Kubo T, Kobayashi M, Ohashi T. Enzyme replacement therapy in two Japanese siblings with Fabry disease, and its effectiveness on angiokeratoma and neuropathic pain. Mol Genet Metab. 2013;110(3):405-410.

9. BIBLIOGRAPHY OF THE CANDIDATE'S PUBLICATIONS

Publications related to the thesis

(Σ IF: 7,447)

Anker P, Fésűs L, Kiss N, Noll J, Becker K, Kuroli E, Mayer B, Bozsányi S, Lőrincz K, Lihacova I, Lihachev A, Lange M, Wikonkál N, Medvecz M. Visualization of Keratin with Diffuse Reflectance and Autofluorescence Imaging and Nonlinear Optical Microscopy in a Rare Keratinopathic Ichthyosis. Sensors (Basel). 2021;21(4):1105. (IF: 3,847)

Anker P, Fésűs L, Kiss N, Lengyel A, Pinti É, Lihacova I, Lihachev A, Plorina EV, Fekete G, Medvecz M. A Cross-Sectional Study of the Dermatological Manifestations of Patients with Fabry Disease and the Assessment of Angiokeratomas with Multimodal Imaging. Diagnostics (Basel). 2023;13(14):2368.

(IF: 3,6)

Publications not related to the thesis

(Σ IF: 17,703)

Kiss N, **Anker P**, Fésűs L, Lőrincz K, Bánvölgyi A, Bozsányi S, Wikonkál N. A rosszindulatú hámeredetű bőrdaganatok kialakulásának genetikai háttere, új ismeretek a karcinogenezis folyamatában. Bőrgy Vener Szeml. 2018; 94:5 pp. 220-226.

Bánvölgyi A, **Anker P,** Lőrincz K, Kiss N, Márton D, Fésűs L, Gyöngyösi N, Wikonkál N. Smoothened receptor inhibitor vismodegib for the treatment of basal cell carcinoma: a retrospective analysis of efficacy and side effects. J Dermatol Treat. 2020; 31(4):387-398. (IF: 3,359)

Kiss N, **Anker P**, Bánvölgyi A, Lőrincz, Fésűs L, Bozsányi S, Szipőcs R, Medvecz M, Wikonkál N. Új képalkotó technikák a bőrgyógyászatban és azok klinikai alkalmazása. Bőrgy Vener Szeml. 2019; 95(3): 90-99.

Bánvölgyi A, **Anker P**, Kiss N, Lőrincz K, Wikonkál N, Medvecz M. Gyulladásos bélbetegségek bőrgyógyászati vonatkozásai – a bél-mikrobiom tükrében. Gasztroent Hep Szeml. 2019; 5(2): 3-7.

Anker P, Medvecz M**.** Ichthyosisok patogenezise: a terminális differenciáció zavarai. Bőrgy Vener Szeml. 2020; 96(1): 3-10.

Farkas K, Bozsányi S, Plázár D, Bánvölgyi A, Fésűs L, **Anker P**, Zakariás S, Lihacova I, Lihachev A, Lange M, Arányi T, Wikonkál NM, Medvecz M, Kiss N. Autofluorescence Imaging of the Skin Is an Objective Non-Invasive Technique for Diagnosing Pseudoxanthoma Elasticum. Diagnostics. 2021; 11(2):260. (IF: 3,992)

Bozsányi S, Farkas K, Bánvölgyi A, Lőrincz K, Fésűs L, **Anker P,** Zakariás S, Jobbágy A, Lihacova I, Lihachev A, Lange M, Bliznuks D, Medvecz M, Kiss N, Wikonkál NM. Quantitative Multispectral Imaging Differentiates Melanoma from Seborrheic Keratosis. Diagnostics (Basel). 2021;11(8):1315. (IF: 3,992)

Haász C, Kuroli E, **Anker P**, Márton DF, Szigeti Á, Nagy Z, Demeter J, Sárdy M, Medvecz M. Periorbitalis bőrtünetekkel járó könnyűlánc-amyloidosis. Orv Hetil. 2021; 162 (32). pp. 1303-1308. (IF: 0,707)

Anker P, Kiss N, Kocsis I, Czemmel É, Becker K, Zakariás S, Plázár D, Farkas K, Mayer B, Nagy N, Széll M, Ács N, Szalai Z, Medvecz M. Report of a Novel ALOX12B Mutation in Self-Improving Collodion Ichthyosis with an Overview of the Genetic Background of the Collodion Baby Phenotype. Life (Basel). 2021;11(7):624. (IF: 3,253)

Pálla S, **Anker P,** Farkas K, Plázár D, Kiss S, Marschalkó P, Szalai Z, Bene J, Hadzsiev K, Maróti Z, Kalmár T, Medvecz M. Co-occurrence of neurofibromatosis type 1 and pseudoachondroplasia - a first case report. BMC Pediatr. 2023 Mar 8;23(1):110. (IF: 2,4)

10. ACKNOWLEDGEMENTS

I must acknowledge those individuals without whom my scientific work would not have been achievable. Foremost, I want to express my appreciation to my supervisor, Márta Medvecz MD PhD. Without her assistance, conducting my research and completing this thesis would not have been possible. Her unwavering support, both professionally and personally, encouraged me throughout my time as a PhD student. Her dedication to research and providing excellent patient care motivated and inspired me. Additionally, I am grateful to Prof. Norbert Wikonkál, who provided me the opportunity to join the Photobiology and Photocarcinogenesis Laboratory as an undergraduate researcher and later as a PhD student. Being a part of this enthusiastic and inspiring research team was truly rewarding.

I would also extend my gratitude to Prof. Péter Holló, who serves as the head of the Department of Dermatology, Venereology, and Dermatooncology at Semmelweis University, and to Prof. Miklós Sárdy, who leads the doctoral program, for their invaluable support during my studies.

I am sincerely thankful to Norbert Kiss MD PhD for his unwavering support, invaluable insights, and constructive criticism, all of which have significantly shaped the current direction of my research and enhanced the quality of my work. Furthermore, I would like to express my appreciation to Kende Lőrincz MD PhD and András Bánvölgyi MD PhD for their assistance and advice during my academic journey.

I want to extend my heartfelt appreciation to the members of our research laboratory, namely Antal Jobbágy MD, Szabolcs Bozsányi MD PhD, Luca Fésűs MD PhD, Klára Farkas MD, Fanni Meznerics MD, Sára Pálla MD and Dóra Plázár MD I am truly grateful for their constant support, guidance, and willingness to help whenever I needed it. Their dedication to scientific work, work ethic, and enthusiasm have been a great source of inspiration for me.

My gratitude goes to Ilze Lihacova, Alexey Lihachev, Emilija Vija Plorina and Marta Lange, as well as the University of Latvia, for their contribution to the development of the MSI device. They have been exceptional collaborative partners throughout these studies, and we have always been able to rely on their support and assistance.

I would like to extend my heartfelt appreciation to Prof. György Fekete MD PhD, Éva Pinti MD, and Anna Lengyel MD, as well as the Pediatric Center, Tűzoltó Street Department, for their ongoing collaboration with patients affected with FD. Your support and dedication have been invaluable, and I am truly grateful for the opportunity to work together.

I am grateful to Judit Knoll MD and Krisztina Becker MD PhD for their invaluable assistance with the EI case study.

I would like to thank Róbert Szipőcs, PhD and the Wigner Research Centre for Physics for the invaluable contribution regarding nonlinear microscopic imaging.

I would like to express my gratitude to Balázs Mayer PhD for his assistance in the genetic verification of the EI patient.

I want to express my heartfelt appreciation to Enikő Kuroli MD for her invaluable contributions to conventional histologic investigations. I would also like to extend special thanks to Edit Szőke and Ivana Pujcseva for their dedicated efforts in preparing the histology slides.

I would also like to express my gratitude to Rita Mátrahegyi for her assistance in capturing the clinical photographs.

Finally, I would like to express my gratitude to my family and friends who have been a constant source of support during my PhD studies.

This work was supported by grants from the National Research, Development and Innovation Office of Hungary - NKFIH (FK_131916, 2019) and EFOP3.6.3-VEKOP-16-2017-00009.